(2)

On Pressure-Shear Plate Impact for Studying the Kinetics of Stress-Induced Phase Transformations

J.C. Escobar and R.J. Clifton

Division of Engineering
Brown University
Providence, RI 02912

Office of Naval Research
Contract N00014-91-J-4169

July 1992

On Pressure-Shear Plate Impact for Studying the Kinetics of Stress-Induced Phase Transformations

J.C. Escobar and R.J. Clifton
Division of Engineering
Brown University
Providence, RI-02912

Abstract

Pressure-shear plate impact experiments are proposed for studying the kinetics of stress-induced phase transformations. The purpose of this paper is to determine loading conditions and specimen orientations which can be expected to activate a single habit plane variant parallel to the impact plane, thereby simplifying the study of the kinetics of the transformation through monitoring the wave profiles associated with the propagating phase boundary. The Wechsler- Lieberman-Read phenomenological theory has been used to determine habit plane indices and directions of shape deformation for a Cu-Al-Ni shape memory alloy which undergoes a martensitic phase transformation under stress. Elastic waves generated by pressure-shear impact have been analyzed for wave propagation in the direction of the normal to a habit plane. A critical resolved shear stress criterion has been used to predict variants which are expected to be activated for a range of impact velocities and relative magnitudes of the normal and transverse components of the impact velocity.

1. Introduction

Recently there has been strong interest in the mathematical modeling of phase boundaries in solids. The boundary between two different phases is modeled as a surface of discontinuity of displacement gradients, strains and stresses. The corresponding boundary value problem in elastostatics has non-unique solutions. Abeyaratne and Knowles (1988) have introduced an additional "kinetic relation" in the form of a constitutive relation which relates the driving traction on the surface of a discontinuity to the velocity of the surface, for the case of quasi–static isothermal motion. With the incorporation of this kinetic relation and a nucleation criterion, the authors are able to obtain unique solutions of the equations of elastostatics. Abeyaratne and Knowles (1990a) extended their study to a three-dimensional body, having elastic or inelastic properties. Thermal and inertial effects

are included in the analysis. In obtaining a kinetic relation, the driving traction is related to the rate of entropy production of the process. In later reports, Abeyaratne and Knowles (1989, 1990b) considered the application of the kinetic relation and the nucleation criterion to the dynamic problem of propagating phase boundaries in solids.

The goal in the present study is to utilize experimental observations to obtain better understanding of the processes occurring during the nucleation and propagation of a phase boundary. Abeyaratne and Knowles have demonstrated the effectiveness of applying an additional constitutive model relating driving force to the velocity of a propagating phase boundary in order to obtain unique solutions to problems such as those described above. The purpose of this study is to obtain a constitutive model of this type based on experimental observation of stress-induced phase transformations. Such a kinetic relation could then be utilized, in analyses such as those described above, to characterize the propagation of phase boundaries in solids. This material characterization can then be applied to such problems as the modeling of shape memory alloys, and transformation toughening of brittle materials.

As a means of understanding the kinetics of stress-induced phase transformations, an ordered shape memory alloy has been chosen for an initial dynamic investigation. Substantial information on this particular alloy is available in the literature, particularly for martensitic transformations induced by quasi–static tensile loading. The specimen to be studied is a Cu-14Al-4Ni (mass%) single crystal, in the DO_3 phase. Upon successful completion of this investigation, the method can be applied to other materials which also undergo phase transformations under stress.

For a material undergoing a martensitic transformation, the plane separating the parent and martensite phases is called the habit plane. The habit plane is a plane of zero distortion, hence any line lying in the plane remains undeformed and unrotated by the transformation. The lattice of the initial (or parent) phase can be related to the lattice of the final (or martensite) phase. There are twelve crystallographically equivalent lattice correspondences for the $\beta_1(DO_3) \rightarrow \beta_1'(18R)$ martensitic transformation considered here. These lattice correspondences are referred to as "correspondence variants" (Saburi and Nenno (1981)). For each of these twelve correspondence variants, there are two crystallographically equivalent habit plane variants, designated by $(+)$ and $(-)$; hence,

there are a total of twenty-four habit plane variants. For a stress-induced martensitic transformation, one or several habit plane variants can be activated, depending on their orientation with respect to the applied load.

Horikawa, et al. (1988) have applied phenomenological theory to study the stress-induced martensitic phase transformation in a Cu-Al-Ni alloy for the case of quasi–static tensile loading. Their results indicate that selection of the habit plane variant is determined by the magnitude of the resolved shear stress in the direction of the projection of the shape deformation onto the habit plane. This result is applied to the present study in an effort to predict the habit plane variant which will be activated by the pressure-shear plate impact experiments. Since the transformation is driven by shear stress, the pressure-shear configuration appears to be the most well suited for the application. Calculations have been carried out for various impact conditions. Results indicate that the impact plane should be inclined at approximately 40 degrees relative to the direction of approach to activate a single variant parallel to the impact plane.

The following sections present the analysis carried out in preparation for the plate impact experiments. Background on the Wechsler-Lieberman-Read (WLR) phenomenological theory is presented in §2. Calculations are reported which predict habit plane indices and directions of the shape deformation for each of the variants for the case of a phase transformation occuring in an unstressed parent material. Results agree to four digits with the values obtained by Horikawa, et al. (1988). The propagation of plane waves in an anisotropic elastic solid are presented in §3. Wave speeds and polarizations for wave propagation perpendicular to a habit plane as well as the jump conditions used to determine the stress state associated with stress wave loading are determined. The analysis is presented for linear elastic response of the crystal; time dependent, dissipative effects associated with the transformation are not included in this initial analysis. In §4 the pressure-shear plate impact experiment is described and the allowable impact conditions for the activation of a single habit plane variant parallel to the impact plane are determined.

2. Application of the Wechsler-Lieberman-Read Phenomenological Theory

The Wechsler-Lieberman-Read (WLR) phenomenological theory (Wechsler, Lieber-

man, Read, 1953) is used in this study to predict habit plane indices and the corresponding directions of shape deformation associated with the martensitic phase transformation of a Cu-Al-Ni alloy. Application of the WLR theory requires prior knowledge of the crystal structures of the parent and martensite phases. This theory has been used in a number of other studies (Otsuka, Wayman, Nakai, Sakamoto, Shimizu, 1976) and (Horikawa, Ichinose, Morii, Miyazaki, Otsuka, 1988) for example, and theoretical results have been found to be consistent with experiment.

Table 1 contains lattice correspondences for $\beta_1(DO_3) \rightarrow \beta_1'$ (18R) martensitic transformation in Cu- 14Al-4Ni (mass%) alloy, where the superscript m denotes components relative to the standard basis for the martensite phase. Vectors represented without the superscript are expressed in terms of the base vectors of the DO_3 phase unless otherwise noted. The correspondences of Table 1 relate three crystal directions in the parent phase (prior to transformation) to three corresponding crystal directions in the martensite phase (after transformation). The crystal structures and a model depicting the structure change are shown schematically in Figure 1, for correspondence variant (4') (Nishiyama and Kajiwara (1963), and Otsuka, et al. (1976)). Figure (1a) is the (DO_3) crystal structure. An expansion or contraction along the principal axes results in the structure in Figure (1b). Uniform shearing on the $\frac{1}{\sqrt{2}}(101)$ plane in the $-\frac{1}{\sqrt{2}}[10\bar{1}]$ direction produces the structure in Figure (1c). Additional shear or shuffle in every third layer results in the final 18R crystal structure shown in (1d) or, referred to orthorhombic axes, in Figure (1e).

In applying the WLR phenomenological theory, the total deformation in the crystal as it undergoes a martensitic transformation is expressed as $\mathbf{F} = \mathbf{R}\mathbf{F}^{\mathbf{s}}\mathbf{U}^{\mathbf{d}}$, where $\mathbf{R}$ is a pure rotation, $\mathbf{F}^{\mathbf{s}}$ is a simple shear, and $\mathbf{U}^{\mathbf{d}}$ is a pure stretch (Nishiyama,1978). Figure (2) depicts schematically the model used to approximate the (DO_3) $\rightarrow$ (18R) structure change. Figure (2a) is the (DO_3) structure. $\mathbf{U}^{\mathbf{d}}$ produces expansion or contraction along the principal axes resulting in the structure shown in (2b). The uniform shear and subsequent shuffle shown in Figures (1c,1d) are approximated by a uniform shear ($\mathbf{F}^{\mathbf{s}}$) of magnitude g, as shown in (2c). In order for the habit plane to remain unrotated by the total deformation, an additional rotation $\mathbf{R}$ is included to rotate the habit plane in (2c) back to the orientation of the habit plane in the (DO_3) phase (2a).

$\mathbf{U}^{\mathbf{d}}$ describes the elongation of the lattice during the transformation. Because the

initial and final crystal structures are known, the components of $\mathbf{U^d}$ are also known. The principal basis vectors, $\mathbf{f}_1$,$\mathbf{f}_2$, $\mathbf{f}_3$, for the lattice deformation $\mathbf{U^d}$ are given in Table 2 for each of the 12 correspondence variants. For the deformation from an initial (DO_3) crystal structure with lattice parameter a_o to the martensite phase (18R crystal structure) with lattice parameters a, b, c, the matrix of components of $\mathbf{U^d}$ relative to the basis $\mathbf{f}_1$,$\mathbf{f}_2$, $\mathbf{f}_3$ is

$$U^d_{ij} = \begin{pmatrix} \sqrt{2}a/a_o & 0 & 0 \\ 0 & b/a_o & 0 \\ 0 & 0 & \sqrt{2}c/9a_o \end{pmatrix}. \tag{2.1}$$

Lattice parameters used are from Horikawa, et al. (1988), namely $a_o = 5.836$Å, $a = 4.382$Å, $b = 5.356$Å, and $c = 38.00$Å.

From knowledge of the crystal structures, the shearing plane and shearing directions can also be obtained and therefore the form of $\mathbf{F^s}$ can be predicted, although the magnitude of the shear is yet to be determined. For the particular crystal considered, shearing is expected to occur on the $\mathbf{f}_3$ plane, in the -$\mathbf{f}_1$ direction. Relative to the **f**-basis, the simple shear takes the form

$$F^s_{ij} = \begin{pmatrix} 1 & 0 & -g \\ 0 & 1 & 0 \\ 0 & 0 & 1 \end{pmatrix} \tag{2.2}$$

where the amount of shearing g is a value to be determined. The total lattice distortion is given by

$$\mathbf{F^d} = \mathbf{F^s U^d}. \tag{2.3}$$

To determine the habit plane, the WLR theory imposes the constraint that the length of a line segment lying in the habit plane remains constant through the transformation. Consider a vector $\mathbf{dX}$ in the habit plane prior to the transformation. After the transformation, the vector is given by

$$\mathbf{dx} = \mathbf{F dX} = (\mathbf{RF^d})\mathbf{dX}. \tag{2.4}$$

The square of the length of the vector is

$$\mathbf{dx} \cdot \mathbf{dx} = \mathbf{dX} \cdot (\mathbf{F^d})^T \mathbf{F^d dX}. \tag{2.5}$$

The requirement that the length of the vector remains unchanged by the transformation, i.e. $\mathbf{dx} \cdot \mathbf{dx} = \mathbf{dX} \cdot \mathbf{dX}$, gives

$$\mathbf{dX} \cdot \mathbf{dX} = \mathbf{dX} \cdot (\mathbf{F^d})^T \mathbf{F^d} \mathbf{dX}. \tag{2.6}$$

For computations, the constraint (2.6) is most conveniently expressed in terms of eigenvalues λ_i^2 and eigenvectors $\mathbf{e}_i$ of $((\mathbf{F^d})^T \mathbf{F^d})$ which satisfy

$$((\mathbf{F^d})^T \mathbf{F^d}) \mathbf{e}_i = \lambda_{\underline{i}}^2 \mathbf{e}_{\underline{i}} \ , \qquad i = 1,\ 2,\ 3 \tag{2.7}$$

where the label symbol $\underline{\ }$ indicates no sum on i. The relation (2.6) becomes

$$\sum_{i=1}^{3} dX_i dX_i = \sum_{i=1}^{3} \sum_{j=1}^{3} dX_i \mathbf{e}_i \cdot (\lambda_j^2 dX_j \mathbf{e}_j) \tag{2.8}$$

or

$$(1 - \lambda_1^2) dX_1^2 + (1 - \lambda_2^2) dX_2^2 + (1 - \lambda_3^2) dX_3^2 = 0 \tag{2.9}$$

where λ_i^2 are the squares of the stretches in the principal directions $\mathbf{e}_i$, and dX_i are initial coordinates (prior to transformation) in the principal basis $\mathbf{e}_i$.

Wechsler, et al. (1953) have shown that a necessary and sufficient condition for a plane of zero distortion to exist is that one of the principal stretches (λ_i) is unity. The sufficiency condition is proven as follows. Take one of the eigenvalues, say $\lambda_1 = 1$. Then from equation (2.9), the relation becomes

$$\frac{dX_2^2}{dX_3^2} = -\frac{1 - \lambda_3^2}{1 - \lambda_2^2}. \tag{2.10}$$

Components dX_2 and dX_3 are proportional while dX_1 spans all values. These requirements on dX_i define a plane which satisfies the condition of zero distortion given by equation (2.9). To prove that one eigenvalue must necessarily equal 1, consider the intersection of

the ellipsoid with the planes $dX_3 = 0, dX_1 = 0, dX_2 = 0$:

$$\begin{aligned} \frac{dX_1^2}{dX_2^2} &= -\frac{1-\lambda_2^2}{1-\lambda_1^2} \\ \frac{dX_2^2}{dX_3^2} &= -\frac{1-\lambda_3^2}{1-\lambda_2^2} \\ \frac{dX_1^2}{dX_3^2} &= -\frac{1-\lambda_3^2}{1-\lambda_1^2}. \end{aligned} \tag{2.11}$$

Assume that $(1-\lambda_1^2)$ is positive. Then the first equation requires that $(1-\lambda_2^2)$ is negative. If $(1-\lambda_2^2)$ is negative, then the second equation requires that $(1-\lambda_3^2)$ be positive. However, if $(1-\lambda_1^2)$ and $(1-\lambda_3^2)$ are both positive, then the third equation is violated. Hence, one of the eigenvalues must be equal to 1.

The eigenvalues λ_i^2 of $(\mathbf{F^d})^T\mathbf{F^d}$ are found by solving the characteristic equation

$$\left|(\mathbf{F^d})^T\mathbf{F^d} - \lambda^2\mathbf{I}\right| = 0 \tag{2.12}$$

where $\mathbf{I}$ is the identity tensor. The resulting expression is a cubic in λ^2; the coefficients of the cubic depend on g. The existence of a plane of zero distortion requires that λ^2=1 is a root. This condition determines the amount of shearing, g. Knowing g one can obtain the remaining two eigenvalues as the remaining two roots of the characteristic equation. The corresponding eigenvectors $\mathbf{e}_i$ can then be determined from equation (2.7).

For $\lambda_1 = 1$ it follows from (2.10) that

$$\frac{dX_2}{dX_3} = \sqrt{\frac{\lambda_3^2 - 1}{1-\lambda_2^2}} = \mp K. \tag{2.13}$$

Equation (2.13) provides the ratio of components dX_2, dX_3 of a vector lying in the habit plane. By taking the cross product of two vectors lying in the plane, the habit plane normal (in the **e**-basis) is found to be

$$\mathbf{n} = \frac{[0, 1, \pm K]}{\sqrt{1+K^2}} \tag{2.14}$$

which are crystallographically equivalent planes for cubic crystals. This equivalence is called degeneracy of the K type. Habit plane normals were found to be of the type

(0.68300, 0.15485, 0.71380) with respect to the base vectors of the DO_3 phase ($\mathbf{a}_1 = [100], \mathbf{a}_2 = [010], \mathbf{a}_3 = [001]$). The components agree to four digits with the results of Horikawa, et al. (1988).

Any vector lying in the habit plane must remain undeformed and unrotated by the transformation. The criterion that vectors in the habit plane remain undeformed by $\mathbf{F^d} = \mathbf{F^s U^d}$ has been used above to determine the habit plane. Although $\mathbf{F^d}$ does not stretch vectors lying in the habit plane, it can rotate such vectors. Therefore, a rotation tensor $\mathbf{R}$ is necessary in the description of the total deformation $\mathbf{F} = \mathbf{R F^s U^d}$ in order to maintain an unrotated habit plane after transformation.

To calculate $\mathbf{R}$ one can use Euler's theorem: " the general displacement of a rigid body with one point fixed is a rotation about some axis" (Goldstein (1980)). To determine the axis of rotation and angle of rotation, consider two vectors $\mathbf{x}$ and $\mathbf{y}$ lying in the habit plane. Define $\mathbf{x'}=\mathbf{F^d x}$ and $\mathbf{y'}=\mathbf{F^d y}$ as the vectors after being rotated by the distortion tensor. From Wayman (1964), the angle of rotation θ and the axis of rotation $\mathbf{u}$ are given by

$$\mathbf{u}\tan(\frac{\theta}{2}) = \frac{(\mathbf{y'}-\mathbf{y})\times(\mathbf{x'}-\mathbf{x})}{(\mathbf{x'}+\mathbf{x})\cdot(\mathbf{y'}-\mathbf{y})} = \frac{(\mathbf{x'}-\mathbf{x})\times(\mathbf{y'}-\mathbf{y})}{(\mathbf{y'}+\mathbf{y})\cdot(\mathbf{x'}-\mathbf{x})}. \tag{2.15}$$

The rotation tensor $\mathbf{R}$ for a rotation $-\theta$ about $\mathbf{u}$ can be expressed conveniently in terms of an orthonormal basis with $\mathbf{u}$ as one of the basis vectors, say $(\mathbf{u}, \mathbf{u'}, \mathbf{u''})$:

$$R^u_{ij} = \begin{pmatrix} 1 & 0 & 0 \\ 0 & \cos\theta & \sin\theta \\ 0 & -\sin\theta & \cos\theta \end{pmatrix}. \tag{2.16}$$

In general, the axis of rotation $\mathbf{u}$ will be inclined with respect to the basis vectors of the DO_3 phase , i.e.

$$\mathbf{u} = u_1\mathbf{a}_1 + u_2\mathbf{a}_2 + u_3\mathbf{a}_3. \tag{2.17}$$

Choose basis vector $\mathbf{u'}$ to lie in the $\mathbf{a}_1, \mathbf{a}_2$-plane, then

$$\mathbf{u'} = \frac{u_2}{\sqrt{u_1^2+u_2^2}}\mathbf{a}_1 - \frac{u_1}{\sqrt{u_1^2+u_2^2}}\mathbf{a}_2, \tag{2.18}$$

and $\mathbf{u}'' = \mathbf{u} \times \mathbf{u}'$, or

$$\mathbf{u}'' = \frac{u_1 u_3}{\sqrt{u_1^2 + u_2^2}}\mathbf{a}_1 + \frac{u_2 u_3}{\sqrt{u_1^2 + u_2^2}}\mathbf{a}_2 - \frac{u_1^2 + u_2^2}{\sqrt{u_1^2 + u_2^2}}\mathbf{a}_3. \tag{2.19}$$

The rotation tensor $\mathbf{R}$ necessary for the habit plane to remain unrotated after the total deformation $\mathbf{F}=\mathbf{R}\mathbf{F}^{\mathbf{s}}\mathbf{U}^{\mathbf{d}}$ then has the following components

$$R^a_{ij} = A_{ki} R^u_{kl} A_{lj}. \tag{2.20}$$

where $\mathbf{A}$ is

$$A_{ij} = \begin{pmatrix} u_1 & u_2 & u_3 \\ \frac{u_2}{\sqrt{u_1^2+u_2^2}} & -\frac{u_1}{\sqrt{u_1^2+u_2^2}} & 0 \\ \frac{u_1 u_3}{\sqrt{u_1^2+u_2^2}} & \frac{u_2 u_3}{\sqrt{u_1^2+u_2^2}} & -\sqrt{u_1^2+u_2^2} \end{pmatrix}. \tag{2.21}$$

The direction $\mathbf{d}$ of the so-called shape deformation (Wayman, (1964)) is the normalized difference between the habit plane normal acted on by $\mathbf{F}$ and the undistorted habit plane normal, i.e.

$$\mathbf{d} = \frac{[\mathbf{F}\mathbf{n} - \mathbf{n}]}{|\mathbf{F}\mathbf{n} - \mathbf{n}|} = \frac{[\mathbf{R}\mathbf{F}^{\mathbf{d}}\mathbf{n} - \mathbf{n}]}{|\mathbf{R}\mathbf{F}^{\mathbf{d}}\mathbf{n} - \mathbf{n}|} \tag{2.22}$$

The direction $\mathbf{d}^p$ of the projection of the shape deformation onto the habit plane is (Otsuka, et al. (1976))

$$\mathbf{d}^p = \frac{[\mathbf{d} - (\mathbf{d}\cdot\mathbf{n})\mathbf{n}]}{|\mathbf{d} - (\mathbf{d}\cdot\mathbf{n})\mathbf{n}|}. \tag{2.23}$$

Experimental results of Horikawa,et al. (1988) show that the activated habit plane variant is the one which maximizes the resolved shear stress in the direction $\mathbf{d}^p$. The direction ($\mathbf{d}^p$) was calculated for each of the variants and is of the type (-0.73041, 0.14455, 0.66753), in the **a**-basis. Table 3 lists the variant number, habit plane normal and the direction of the projection of the shape deformation onto the habit plane, calculated as described above.

3. Plane Waves in Elastic Anisotropic Media

3.1 Governing Equations

The balance of linear momentum (no body forces) gives

$$\sigma_{ij,j} = \rho \ddot{u}_i \tag{3.1}$$

where $\boldsymbol{\sigma}$ is the stress tensor, ρ is the mass density, and $\mathbf{u}$ is the displacement. From conservation of angular momentum, the stress tensor is symmetric, i.e. $\sigma_{ij} = \sigma_{ji}$. For a linear elastic material the stress-strain relation is given by

$$\sigma_{ij} = C_{ijkl}\epsilon_{kl} \tag{3.2}$$

with strain components $\boldsymbol{\epsilon}$ given by

$$\epsilon_{ij} = \frac{1}{2}(u_{i,j} + u_{j,i}). \tag{3.3}$$

$\mathbf{C}$ is a fourth order tensor which represents the elastic stiffness of the medium. The stiffness tensor has the symmetries $C_{ijkl} = C_{jikl}, C_{ijkl} = C_{ijlk}$; materials for which the stress is derivable from a strain energy function have the additional symmetry $C_{ijkl} = C_{klij}$. In general, $\mathbf{C}$ can have 21 independent components. However, in a cubic material the number of independent constants is reduced to three. (e.g. Musgrave, 1970)

Alternatively, the components of stress and strain can be expressed as six-dimensional vectors. The corresponding stiffness matrix $\mathbf{C}$ is a second order tensor. The stress-strain relation is then given by

$$\sigma_p = C_{pq}\epsilon_q \tag{3.4}$$

where

$$\boldsymbol{\sigma} = \begin{pmatrix} \sigma_1 \\ \sigma_2 \\ \sigma_3 \\ \sigma_4 \\ \sigma_5 \\ \sigma_6 \end{pmatrix} = \begin{pmatrix} \sigma_{11} \\ \sigma_{22} \\ \sigma_{33} \\ \sigma_{23} \\ \sigma_{13} \\ \sigma_{12} \end{pmatrix}, \qquad \boldsymbol{\epsilon} = \begin{pmatrix} \epsilon_1 \\ \epsilon_2 \\ \epsilon_3 \\ \epsilon_4 \\ \epsilon_5 \\ \epsilon_6 \end{pmatrix} = \begin{pmatrix} \epsilon_{11} \\ \epsilon_{22} \\ \epsilon_{33} \\ 2\epsilon_{23} \\ 2\epsilon_{13} \\ 2\epsilon_{12} \end{pmatrix} \tag{3.5}$$

and, for a cubic material, **C** has the form

$$C_{ij} = \begin{pmatrix} C_{11} & C_{12} & C_{12} & 0 & 0 & 0 \\ C_{12} & C_{11} & C_{12} & 0 & 0 & 0 \\ C_{12} & C_{12} & C_{11} & 0 & 0 & 0 \\ 0 & 0 & 0 & C_{44} & 0 & 0 \\ 0 & 0 & 0 & 0 & C_{44} & 0 \\ 0 & 0 & 0 & 0 & 0 & C_{44} \end{pmatrix}. \tag{3.6}$$

The components of the second-order tensor are related to the components of the four-tensor by

$$C_{11} = C_{1111} = C_{2222} = C_{3333}$$

$$C_{12} = C_{1122} = C_{2233} = C_{3311}, \text{etc.}$$

$$C_{44} = C_{2323} = C_{3131} = C_{1212}, \text{etc.}$$

3.2 Principal Directions of Wave Propagation

For elastic wave propagation in an anisotropic material, the polarization of the wave (i.e. the direction of the jump in particle velocity across the wave front) will not, in general, be perpendicular to the direction of propagation (longitudinal wave), nor will it be parallel to the direction of propagation (shear wave). Rather, the polarization will be *predominantly* perpendicular to the propagation direction (quasi-longitudinal) or *predominantly* parallel to the propagation direction (quasi-shear). There are, however, certain directions in which purely longitudinal and purely shear waves propagate. These directions, called principal directions, can be determined by crystal symmetry. From Hadamard's result (Hadamard (1903)) that for a given direction of wave propagation, the polarization vectors for the three types of waves are mutually orthogonal it follows that principal directions for purely longitudinal waves are also principal directions for purely shear waves.

The crystal structure considered here (parent phase) is a cubic with 432 symmetry. According to Auld (1990), the principal directions of propagation are along the 2-fold, 3-fold, and 4-fold axes of rotational symmetry. Therefore, the principal directions are the ⟨110⟩, ⟨111⟩ and ⟨100⟩ type crystallographic directions, respectively. Along the 2-fold axis ⟨110⟩, the shear waves may or may not be degenerate, i.e. have the same wave speed. Along the 3-fold ⟨111⟩ and 4-fold ⟨100⟩ axes, the two shear modes are degenerate. For crystals with cubic symmetry, Table 4 gives the principal directions **n**, the corresponding

polarizations **p** and the wave speeds c (Auld (1990), and (A9) of Appendix). Suezawa and Sumino (1976) have shown that the elastic properties of the Cu-Al- Ni crystals considered here are dependent on the temperature at which the samples are quenched. Elastic constants at room temperature, for samples which have been water quenched at 0°C, are determined to be C_{11} = 141.76 GPa, C_{12} = 126.24 GPa, C_{44} = 97.0 GPa. Wavespeeds for these elastic constants and the theoretical mass density ρ = 7100kg/m^3 are also given in Table 4.

In the present study, wave propagation in the direction of the habit plane normal is considered. The polarization vectors and corresponding wave speeds in an unstressed parent material have been determined for variant 3′(+) ((A9) of Appendix). The quasi-longitudinal wave has polarization vector [0.689901, 0.682925, 0.240105] and wavespeed 5704 m/s. The quasi-shear waves have polarization vectors [-0.165363, -0.174236, 0.97072] and [0.704764, -0.709405, -0.007275] and wave speeds 3553 m/s and 1187 m/s, respectively.

3.3 Jump Conditions

Let the jump in particle velocity across a wavefront separating regions i and j be denoted by

$$[\mathbf{v}]^{i,j} = \mathbf{v}^j - \mathbf{v}^i \tag{3.7}$$

where $\mathbf{v}^j, \mathbf{v}^i$ are the particle velocities as the wavefront is approached from regions j and i, respectively. The jump in particle velocity across a wavefront separating region i and region j can be written as

$$[\mathbf{v}]^{i,j} = a^{i,j}\mathbf{p}^{i,j} \tag{3.8}$$

where $\mathbf{p}^{i,j}$ is the polarization of the wave and $a^{i,j}$ is the amplitude of the wave.

The jump in stress across a wavefront is given by

$$[\boldsymbol{\sigma}]^{i,j} = a^{i,j}\mathbf{S}^{i,j}, \tag{3.9}$$

where $\mathbf{S}^{i,j}$ is the stress polarization vector of a wavefront separating region i and region j.

For cubic crystals, the stress polarization vector can be expressed as (Appendix A)

$$\mathbf{S}^{i,j} = -\frac{1}{c}\begin{pmatrix} C_{11}n_1p_1 + C_{12}(n_2p_2 + n_3p_3) \\ C_{11}n_2p_2 + C_{12}(n_3p_3 + n_1p_1) \\ C_{11}n_3p_3 + C_{12}(n_1p_1 + n_2p_2) \\ C_{44}(n_2p_3 + n_3p_2) \\ C_{44}(n_3p_1 + n_1p_3) \\ C_{44}(n_1p_2 + n_2p_1) \end{pmatrix} \tag{3.10}$$

where c is the velocity of wave propagation, and n_i, p_i are the components of the direction of wave propagation and the polarization vector, respectively.

4. Experiment Design

In the proposed experiment, pressure-shear plate impact will be used to generate quasi-longitudinal and quasi-shear plane waves in the specimen. The experiment is designed to induce a martensitic phase transformation resulting in a single crystallographic variant with a phase boundary propagating in the direction normal to the impact plane. The activation of only a single variant will simplify the interpretation of measured wave profiles to obtain information on the kinetics of the phase transformation.

4.1 Pressure-shear Plate Impact Experiments

The pressure-shear plate impact experiment is shown schematically in Figure 3. The particular experiment considered here is that of symmetric impact, in which the flyer and target (specimen) are made from the same material (e.g. Gilat and Clifton (1985)). The flyer and target are inclined relative to the direction of approach of the projectile. Upon impact, both longitudinal and shear waves are generated. These waves propagate into the flyer and target plates. Interferometry is used to monitor the wave profiles at the rear surface of the target plate. A normal velocity interferometer (NVI) detects changes in velocity normal to the specimen surface and is used to monitor the longitudinal component of the velocity-time profile. A transverse displacement interferometer (TDI) is used to monitor the in-plane motion of the rear surface of the target and thus is used to obtain the shear components of the velocity-time profile. The interferometry set-up commonly used is shown in Figure 4 (Kim, Clifton and Kumar (1977)). Because the normal to the habit plane is not a principal direction of wave propagation, the motion associated

with the transformation will cause a three-dimensional motion of the rear surface of the specimen. Therefore, the experimental set-up used in this study will incorporate a normal velocity interferometer and two transverse displacement interferometers. The two TDIs will be oriented perpendicular to one another in order to obtain complete information on the in-plane displacement.

For this project, there will be additional wave structure associated with the martensitic transformation and the propagating phase boundary. The phase boundary is expected to propagate at a fraction of the shear wave speed. The relative arrival times of the quasi-longitudinal and quasi-shear waves at the rear surface of the specimen is shown schematically in a time-distance diagram in Figure 5. For this diagram, the phase boundary is assumed to stop propagating when it meets the longitudinal unloading wave reflected from the rear surface of the target plate. Other possibilities exist. For example, the phase boundary may continue to propagate in the forward direction or may reverse direction depending on the loading conditions.

The existence of a propagating phase boundary, and the velocity of propagation of the boundary, will be determined from comparison of measured normal and transverse components of the free-surface velocity with those predicted by elastic wave theory. The principal wave for determining the velocity of the phase boundary is the slowest shear wave. The wave profiles and the velocity of propagation of the phase boundary will provide information on the kinetics of the transformation.

4.2 State of Stress

The state of stress and the particle velocity in the material can be expressed in terms of jumps across wavefronts propagating through the material. The magnitudes are related to the velocity of the incident projectile.

The configuration considered is that of symmetric impact. A schematic of the specimen orientation is shown in Figure (6a). The normal to the impact plane coincides with the habit plane normal ($\mathbf{n}$) of the variant to be activated. Furthermore, the specimen is oriented such that shearing is in the direction ($\mathbf{d}^p$) of the projection of the shape deformation onto the habit plane associated with the martensitic transformation of the variant to be activated. From the geometry of the problem the normal and transverse components

of the projectile velocity are, respectively,

$$\begin{aligned} u_o &= V_o \cos\theta \\ v_o &= V_o \sin\theta \end{aligned} \tag{4.1}$$

where θ is the skew angle of the impact (i.e. the angle of inclination of the normal to the impact plane relative to the direction of approach). The velocity $\mathbf{V}_o$ of the projectile can be represented as

$$\mathbf{V}_o = u_o\mathbf{n} - v_o\mathbf{d}^{\mathbf{P}}. \tag{4.2}$$

Upon impact, quasi-longitudinal and quasi-shear waves are generated which propagate into the two materials (target and flyer). The direction of wave propagation is normal to the specimen surface and hence normal to the habit plane of the variant to be activated. The quasi-longitudinal wave has wave speed c_1. The quasi-shear waves have wave speeds c_2 and c_3 with $c_2 \geq c_3$. The wave speed of the propagating phase boundary is denoted by c_p. Consider Figure (6b). The polarization vector of the longitudinal wave causing the jump in particle velocity from region 4^- to region 3^- will be denoted as $\mathbf{p}^{4^-,3^-}$. The amplitude of the jump in particle velocity across this wavefront will be denoted $a^{4^-,3^-}$. Let P^+ be a point on the target side of the impact plane and P^- be the corresponding point on the flyer side of the impact plane. The velocities at P^+ and P^- can be expressed as the jumps in velocity across successive wavefronts, i.e.

$$\begin{aligned} \mathbf{v}^{P^-} &= \mathbf{V}_o + a^{4^-,3^-}\mathbf{p}^{4^-,3^-} + a^{3^-,2^-}\mathbf{p}^{3^-,2^-} + a^{2^-,1^-}\mathbf{p}^{2^-,1^-} + a^{1^-,0^-}\mathbf{p}^{1^-,0^-} \\ \mathbf{v}^{P^+} &= \mathbf{0} + a^{4^+,3^+}\mathbf{p}^{4^+,3^+} + a^{3^+,2^+}\mathbf{p}^{3^+,2^+} + a^{2^+,1^+}\mathbf{p}^{2^+,1^+} + a^{1^+,0^+}\mathbf{p}^{1^+,0^+}. \end{aligned} \tag{4.3}$$

Due to the symmetry of the problem, the polarization vectors satisfy $\mathbf{p}^{j^-,k^-} = -\mathbf{p}^{j^+,k^+} \equiv -\mathbf{p}^{j,k}$ and the amplitudes satisfy $a^{j^-,k^-} = a^{j^+,k^+} \equiv a^{j,k}$. The last terms in equations (4.3) represent the jump in particle velocity across the phase boundary; $a^{1,0}\mathbf{p}^{1,0} \equiv [\mathbf{v}]_b$ where $[\mathbf{v}]_b = -c_p[\nabla\mathbf{u}]\mathbf{n}$ (Appendix B). Define the polarization of the phase boundary to be $\mathbf{p}^{\mathbf{b}} = \mathbf{p}^{1,0} \equiv [\mathbf{v}]_b/c_p = -[\nabla\mathbf{u}]\mathbf{n} = -[\mathbf{F} - \mathbf{I}]\mathbf{n}$. From the continuity of the particle velocity across the impact plane (*i.e.* $\mathbf{v}^{P^-} = \mathbf{v}^{P^+}$), the amplitudes of the

jumps are

$$a^{4,3} = \frac{1}{2}\mathbf{V_o} \cdot \mathbf{p}^{4,3} - c_p \mathbf{p}^b \cdot \mathbf{p}^{4,3}$$
$$a^{3,2} = \frac{1}{2}\mathbf{V_o} \cdot \mathbf{p}^{3,2} - c_p \mathbf{p}^b \cdot \mathbf{p}^{3,2} \tag{4.4}$$
$$a^{2,1} = \frac{1}{2}\mathbf{V_o} \cdot \mathbf{p}^{2,1} - c_p \mathbf{p}^b \cdot \mathbf{p}^{2,1}.$$

From equation (3.9), the jump in stress is related directly to the jump in particle velocity. Therefore, the stress state in region Q is given by

$$\boldsymbol{\sigma}^Q = \mathbf{0} + a^{4,3}\mathbf{S}^{4,3} + a^{3,2}\mathbf{S}^{3,2} + a^{2,1}\mathbf{S}^{2,1} \tag{4.5}$$

where $\mathbf{S}^{4,3}$ is the stress polarization vector of the quasi-longitudinal wave and $\mathbf{S}^{3,2}$ and $\mathbf{S}^{2,1}$ are stress polarization vectors for the quasi-shear waves. For non-degenerate shear waves, the stress state in region R after the quasi-longitudinal wave and one quasi-shear wave passes, but prior to the arrival of the second quasi-shear wave is

$$\boldsymbol{\sigma}^R = \mathbf{0} + a^{4,3}\mathbf{S}^{4,3} + a^{3,2}\mathbf{S}^{3,2}. \tag{4.6}$$

Also, prior to the arrival of any shear waves, the stress state in region S is given by

$$\boldsymbol{\sigma}^S = \mathbf{0} + a^{4,3}\mathbf{S}^{4,3}. \tag{4.7}$$

4.3 Numerical Results

Calculations have been carried out in accordance with sections 2,3 and 4.2 to determine the best impact conditions for achieving the activation of a single variant with normal parallel to the impact plane. It is important that the transformation is not induced until the second quasi-shear wave arrives, in order to simplify analysis of the experimental results.

From (4.4) the amplitudes $a^{2,1}, a^{3,2}$, and $a^{4,3}$ can be calculated for assumed values of c_p. (The assumption that the polarization vector, $\mathbf{p}^b$, of the phase boundary can be approximated by the polarization vector for a phase transformation of the unstressed material is considered in Appendix C.) As mentioned previously, Horikawa, et al. (1988)

found that selection of a habit plane variant was determined by the highest resolved shear stress (RSS) on the habit plane in the direction of the projection of the shape deformation onto the habit plane. For transformation of this alloy near room temperature, they found the critical RSS (CRSS) at transformation to be approximately 50 MPa. In order to determine suitable impact conditions, this criterion for transformation has been adopted here. Calculation of the stress state from (4.5) and the resolved shear stress from (C1), and the application of the empirical results of Horikawa, et al. (1988) provides a basis for predicting which variants will most likely be activated by the imposed stress.

Calculations of the resolved shear stress on each of the habit planes have been carried out for a variety of impact conditions. The purpose is to determine conditions for which only the variant with its habit plane parallel to the impact plane is induced (i.e. the RSS for this variant equals the critical value of the resolved shear stress necessary for activation of a variant and this value is significantly higher than the RSS on all other variants). In these calculations, the crystals are assumed to be oriented with the $3'(+)$ habit plane parallel to the specimen surface. The specimen is inclined to the direction of propagation of the flyer by an angle θ. The shearing direction $\mathbf{d}^p$ is the direction of the projection of the shape deformation onto the habit plane.

Calculations were carried out using equations (4.5)-(4.7) for a variety of impact angles and impact velocities. The plates were taken to be inclined at various angles θ between 0 and 45 degrees. At low angles, the resolved shear stress on the $3'(+)$ habit plane was lower than the resolved shear stress on other habit planes. Table 5 contains results for normal impact loading ($\theta = 0$), incident velocity $V_o = 35$ m/s, and phase boundary velocities $c_p = 0$, 2.5, 5m/s. Table 6 contains similar results for $\theta = 20$ deg., $V_o = 30$ m/s. The calculations for $c_p = 0$ m/s is carried out in order to determine whether the stress state produced by the quasi- longitudinal and quasi-shear waves will result in a critical level of the resolved shear stress on any of the variants. Calculations for $c_p \geq 0$ m/s are carried out in order to probe the effect of a propagating phase boundary on the corresponding stress state. Columns of values for quasi-longitudinal and quasi-shear waves are labeled, respectively L(1), T(2), and T(3) (T denotes transverse). Values of the resolved shear stress in columns labeled L(1) correspond to the stress state after the arrival of the quasi-longitudinal wave (1) but prior to the arrival of either quasi-shear wave. Values of the

RSS in columns labeled T(2) and T(3) correspond to the stress states after the first shear wave (2) arrives and after the second shear wave (3) arrives, respectively. In each case, the resolved shear stress on other variants was higher than the resolved shear stress on the habit plane of variant $3'(+)$. Therefore, it can be concluded that for small skew angles such as $\theta = 20$ degrees, the desired habit plane variant $3'(+)$ will not be activated.

Tables 7, 8 and 9 contain values of the RSS obtained for skew angles θ = 35, 40, 45 degrees, respectively, for incident velocity V_o = 20 m/s, and phase boundary velocities c_p = 0, 2.5, 5m/s. For each of these angles, the highest resolved shear stress is on the $3'(+)$ habit plane, with the next highest resolved shear stress on the $6'(-)$ habit plane. Also, for each of these skew angles, the highest resolved shear stress is significantly greater than the next highest value of resolved shear stress. Consider c_p = 0 m/s; for θ = 35 deg., the RSS on variant $3'(+)$ is 14.6% greater than the RSS on variant $6'(-)$. For θ = 40 and 45 deg., this value is 20.3% and 25.0%, respectively. For increasing c_p, this value decreases as the resolved shear stress on each of these habit planes decreases. Figure 7 shows the resolved shear stress for each of the variants in bar-graph form (θ = 40 deg., V_o = 20 m/s, c_p = 5 m/s). The empty bars represent the magnitude of the resolved shear stress for each variant after the quasi-longitudinal and first quasi-shear wave passes. The filled bars represent the magnitude of the resolved shear stress after the second shear wave passes. Figure 8 shows the variation with phase boundary velocity of the amplitudes of the jumps in particle velocity across the wavefronts. Each of these amplitudes varies linearly with the velocity of the phase boundry, c_p, from (4.4) when $\mathbf{p}^b$ is taken to be a constant. For $\mathbf{p}^b$ not equal to a constant, $a^{i,j}$ are non-linear functions of c_p, however this additional dependence on c_p is expected to be weak ((C9) of Appendix C). Therefore, the magnitudes of the jumps in particle velocity at the rear surface of the specimen associated with the arrival of the quasi-longitudinal and quasi-shear waves are a direct measure of the phase boundary velocity. From Figure 8, it is apparent that the amplitude $a^{2,1}$ is the most strongly dependent on c_p. This result is expected since the polarization of the wave with amplitude $a^{2,1}$ is very nearly in the direction $\mathbf{d}^p$ of the projection of the shape deformation onto the habit plane.

If the transformation does not occur as expected at the stress states considered, then the incident projectile velocity can be increased in order to increase the resolved shear stress on the habit plane to be induced. For example, Table 10 contains values of the RSS

on each of the variants for $\theta = 40$ deg. and incident velocity $V_o = 30$ m/s. It is clear that the RSS on the $3'(+)$ habit plane is significantly larger than for incident velocity $V_o = 20$ m/s.

In order to activate only a single variant, the most desirable orientations are those in which the resolved shear stress for a single variant is significantly higher than that of all the other variants. The variant to be activated in these experiments is variant $3'(+)$ which will be parallel to the impact plane and hence normal to the direction of propagation of the elastic waves and the phase boundary. Therefore, specimen orientations which will be obtained and tested have plate normals in the [0.71380, 0.68300,0.15485] crystallographic direction. The inclination, θ, of the impact plane relative to the direction of approach will be near 40 deg. in order to obtain a significantly greater resolved shear stress on the habit plane of the $3'(+)$ variant than on any other variant.

5. Conclusions

The previous sections describe analysis and calculations carried out in preparation for proposed experiments to study the kinetics of stress-induced phase transformations. A single crystal of a shape memory alloy, Cu-14Al-4Ni (mass%), DO_3 phase, has been chosen for the preliminary dynamic investigation. Loading conditions and specimen orientations necessary to generate stress waves which induce only a single habit plane variant parallel to the impact plane are determined. In doing so, calculations based on phenomenological theory have been carried out to determine habit plane normals and directions of shape deformation corresponding to each of the 24 habit plane variants. The polarization vectors associated with the propagating phase boundary and the corresponding wave speeds have been determined for waves propagating in an unstressed parent material. Stress polarization vectors have been obtained for an anisotropic, cubic material determined in terms of the direction of wave propagation, the polarization, and material properties. The stress state due to plate impact loading is calculated for a variety of impact conditions. The specimens are assumed to be oriented such that the direction of wave propagation is normal to the habit plane of variant $3'(+)$. Results of previous investigators have indicated that, for the case of quasi-static tensile loading, activation of a particular variant is dependent on the resolved shear stress on the habit plane in the direction of the projection of the shape deformation onto the habit plane. The results described above were used to determine

such values of RSS on each of the habit planes for the loading conditions considered. For pressure-shear plate impact, inclination of the impact plane by approximately 40 degrees, relative to the direction of approach of the projectile, provides the more favorable impact conditions for activation of variant $3'(+)$ only.

Specimens of this Cu-Al-Ni alloy are being obtained with specimen normals parallel to the (0.71380, 0.68300,0.15485) crystallographic direction. One apparently vital aspect of the specimen preparation and resulting material properties appears to be the temperature at which the samples are quenched (Suezawa and Sumino (1976)). Therefore, in order to obtain crystals with elastic properties similar to those reported for other investigations referred to in this report, the crystals obtained will be quenched at 273 K. A new interferometry set-up is being designed to incorporate a normal velocity interferometer (NVI) with two transverse displacement interferometers (TDI). The TDIs are oriented to monitor displacements in mutually perpendicular directions to record both in-plane displacement components, which result because the normal to the habit plane is not a principal direction for elastic wave propagation in these crysstals.

References

Abeyaratne, R. and Knowles, J.K. (1988),"On the Dissipative Response Due to Discontinuous Strains in Bars of Unstable Elastic Material,"*Int. J. Solids Structures*, **24**, 1021-1044.

Abeyaratne, R. and Knowles, J.K. (1989),"Kinetic Relations and the Propagation of Phase Boundaries in Solids," Cal.-Tech. Technical Report No. 10, ONR Contract N00014-87-K-0117.

Abeyaratne, R. and Knowles, J.K. (1990a), "On the Driving Traction Acting on a Surface of Discontinuity in a Continuum," *J. Mech. Phys. Solids*, **38**, 345-360.

Abeyaratne, R. and Knowles, J.K. (1990b), "Implications of Viscosity and Strain-gradient Effects for the Kinetics of Propagating Phase Boundaries in Solids," Cal.-Tech. Technical Report No. 11, ONR Contract N00014-87-K-0117.

Auld, B.A. (1990), *Acoustic Fields and Waves in Solids*, vol. I, Robert E. Krieger Publishing Co., Malabar, FL.

Courant, R. and Hilbert, D. (1962), *Methods of Mathematical Physics, Volume II: Partial Differential Equations*, John Wiley & Sons, New York.

Gilat, A. and Clifton, R.J. (1985), "Pressure-Shear Waves in 6061-T6 Aluminum and Alpha-Titanium," *J. Mech. Phys. Solids*, **33**, 263-284.

Goldstein, H.(1980), *Classical Mechanics*, 2nd Ed., Addison-Wesley Publishing Co., Reading, MA.

Hadamard, J. (1903), *Lecons sur la Propagation des Ondes et les Equations de l'Hydrodynamique*, Paris.

Horikawa, H., Ichinose, S., Morii, K., Miyazaki, S., and Otsuka, K. (1988), "Orientation Dependence of $\beta_1 \rightarrow \beta_1'$ Stress-Induced Martensitic Transformation in a Cu- Al-Ni Alloy," *Metall. Trans. A*, **19A**, 915-923.

Kim, K.S., Clifton, R.J., and Kumar, P. (1977), " A Combined Normal and Transverse Displacement Interferometer with an Application to Impact of Y-Cut Quartz," *J. Appl. Phys.*, **48**, 4132- 4139.

Musgrave, M.J.P. (1970), *Crystal Acoustics*, Holden-Day, San Francisco.

Nishiyama, Z. (1978), *Martensitic Transformation*, Academic Press, New York.

Nishiyama, Z. and Kajiwara,S. (1963), "Electron Microscope Study of the Crystal Structure of the Martensite in a Copper-Aluminum Alloy," *Jap. J. Appl. Phys.*, **2**, 478-486.

Otsuka,K., Wayman, C.M., Nakai, K., Sakamoto, H., Shimizu, K. (1976), "Superelasticity Effects and Stress-Induced Martensitic Transformations in Cu-Al-Ni Alloys," *Acta Metall.*, **24**, 207-226.

Saburi, T., and Nenno, S. (1981), "The Shape Memory Effect and Related Phenomena," in *Proc. Int. Conf. Solid-Solid Phase Transformations*, H.I. Aaronson, D.E. Laughlin, R.E. Sekerka, and C.M. Wayman, eds., Pittsburgh, PA, 1455-1479.

Suezawa, M. and Sumino, K. (1976), "Behaviour of Elastic Constants in Cu-Al-Ni Alloy in the Close Vicinity of Ms-point," *Scripta Metall.*, **10**, 789-92.

Wayman, C.M. (1964), *Introduction to the Crystallography of Martensite Transformation*, Macmillan Series in Material Science, New York.

Wechsler,M.S., Lieberman, D.S., and Read, T.A. (1953), "On the Theory of the Formation of Martensite," *Trans. AIME*, **197**, 1503-1515.

Appendix A: Determination of the Stress Polarization Vector

Consider the balance of linear momentum in the following form:

$$\begin{pmatrix} \rho & 0 & 0 \\ 0 & \rho & 0 \\ 0 & 0 & \rho \end{pmatrix} \begin{pmatrix} v_1 \\ v_2 \\ v_3 \end{pmatrix}_t + \begin{pmatrix} -1 & 0 & 0 & 0 & 0 & 0 \\ 0 & 0 & 0 & 0 & 0 & -1 \\ 0 & 0 & 0 & 0 & -1 & 0 \end{pmatrix} \begin{pmatrix} \sigma_1 \\ \sigma_2 \\ \sigma_3 \\ \sigma_4 \\ \sigma_5 \\ \sigma_6 \end{pmatrix}_{x_1}$$

$$+ \begin{pmatrix} 0 & 0 & 0 & 0 & 0 & -1 \\ 0 & -1 & 0 & 0 & 0 & 0 \\ 0 & 0 & 0 & -1 & 0 & 0 \end{pmatrix} \begin{pmatrix} \sigma_1 \\ \sigma_2 \\ \sigma_3 \\ \sigma_4 \\ \sigma_5 \\ \sigma_6 \end{pmatrix}_{x_2}$$

$$+ \begin{pmatrix} 0 & 0 & 0 & 0 & -1 & 0 \\ 0 & 0 & 0 & -1 & 0 & 0 \\ 0 & 0 & -1 & 0 & 0 & 0 \end{pmatrix} \begin{pmatrix} \sigma_1 \\ \sigma_2 \\ \sigma_3 \\ \sigma_4 \\ \sigma_5 \\ \sigma_6 \end{pmatrix}_{x_3} = \begin{pmatrix} 0 \\ 0 \\ 0 \\ 0 \\ 0 \\ 0 \end{pmatrix}$$

or

$$\mathbf{M}\mathbf{v}_t + \mathbf{B}_i \boldsymbol{\sigma}_{x_i} = \mathbf{0} \qquad (A1)$$

where $v_i = u_{i,t}$. The constitutive equation is given by $\boldsymbol{\sigma} = \mathbf{C}\boldsymbol{\epsilon}$, where $\mathbf{C}$ is the stiffness tensor. Therefore,

$$\boldsymbol{\sigma}_t = \mathbf{C}\boldsymbol{\epsilon}_t. \qquad (A2)$$

The strain rate is given by

$$(\epsilon_{ij})_t = \frac{1}{2}(v_{i,j} + v_{j,i});$$

alternatively,

$$\begin{pmatrix} \epsilon_1 \\ \epsilon_2 \\ \epsilon_3 \\ \epsilon_4 \\ \epsilon_5 \\ \epsilon_6 \end{pmatrix}_t = \begin{pmatrix} 1 & 0 & 0 \\ 0 & 0 & 0 \\ 0 & 0 & 0 \\ 0 & 0 & 0 \\ 0 & 0 & 1 \\ 0 & 1 & 0 \end{pmatrix} \begin{pmatrix} v_1 \\ v_2 \\ v_3 \end{pmatrix}_{x_1} + \begin{pmatrix} 0 & 0 & 0 \\ 0 & 1 & 0 \\ 0 & 0 & 0 \\ 0 & 0 & 1 \\ 0 & 0 & 0 \\ 1 & 0 & 0 \end{pmatrix} \begin{pmatrix} v_1 \\ v_2 \\ v_3 \end{pmatrix}_{x_2} + \begin{pmatrix} 0 & 0 & 0 \\ 0 & 0 & 0 \\ 0 & 0 & 1 \\ 0 & 1 & 0 \\ 1 & 0 & 0 \\ 0 & 0 & 0 \end{pmatrix} \begin{pmatrix} v_1 \\ v_2 \\ v_3 \end{pmatrix}_{x_3}$$

or

$$\epsilon_t = -\mathbf{B}_i^T \mathbf{v}_{x_i}. \tag{A3}$$

From (A2) and (A3):

$$\mathbf{C}^{-1}\boldsymbol{\sigma}_t = -\mathbf{B}_i^T \mathbf{v}_{x_i}. \tag{A4}$$

Combining equations (A1) and (A4) one obtains

$$\left(\begin{array}{c|c} \mathbf{M} & \mathbf{0} \\ \hline \mathbf{0} & \mathbf{C}^{-1} \end{array}\right)\left(\begin{array}{c} \mathbf{v} \\ \hline \boldsymbol{\sigma} \end{array}\right)_t + \left(\begin{array}{c|c} \mathbf{0} & \mathbf{B}_i \\ \hline \mathbf{B}_i^T & \mathbf{0} \end{array}\right)\left(\begin{array}{c} \mathbf{v} \\ \hline \boldsymbol{\sigma} \end{array}\right)_{x_i} = \left(\begin{array}{c} \mathbf{0} \\ \hline \mathbf{0} \end{array}\right)$$

or

$$\mathbf{A}^t \mathbf{w}_t + \mathbf{A}^i \mathbf{w}_{x_i} = \mathbf{0}. \tag{A5}$$

Equation (A5) represents a system of linear, symmetric, hyperbolic, partial differential equations for the vector $\mathbf{w}$ composed of the particle velocity $\mathbf{v}$ and the stress $\boldsymbol{\sigma}$ (e.g. Courant and Hilbert, (1962)). The equations governing the propagation of discontinuities in $\mathbf{w}$, as required for the step loading of the plate impact experiments, are the same as those governing the propagation of acceleration waves for which $\mathbf{w}$ is continuous but has discontinuous derivatives. Thus the analysis can be presented in terms of acceleration waves for which the principal results are obtained immediately by considering a wave front $\phi = ct - \mathbf{n} \cdot \mathbf{x}$ for a wave propagating in direction $\mathbf{n}$ with speed c. The resulting equation for the jump in the derivative $\mathbf{w}_\phi$ across the wave front ϕ = constant is

$$(\mathbf{A}^t \phi_t + \mathbf{A}^i \phi_{x_i})[\mathbf{w}_\phi] = \mathbf{0}, \tag{A6}$$

or

$$(c\mathbf{A}^t + -n_i \mathbf{A}^i)[\mathbf{w}_\phi] = \mathbf{0}, \tag{A7}$$

which has the form

$$\left(\begin{array}{c|c} c\mathbf{M} & -n_i \mathbf{B}_i \\ \hline -n_i \mathbf{B}_i^T & c\mathbf{C}^{-1} \end{array}\right)\left(\begin{array}{c} [\mathbf{v}] \\ \hline [\boldsymbol{\sigma}] \end{array}\right) = \left(\begin{array}{c} \mathbf{0} \\ \hline \mathbf{0} \end{array}\right). \tag{A8}$$

In writing (A8) from (A7) $[\mathbf{v}_\phi]$ and $[\boldsymbol{\sigma}_\phi]$ have been replaced by $[\mathbf{v}]$ and $[\boldsymbol{\sigma}]$, respectively, because of the previously mentioned equivalence, for the linear system (A5), of the equations

governing the propagation of discontinuities in $\mathbf{w}$ and those governing the propagation of discontinuities in the derivative $\mathbf{w}_\phi$. The equation governing the wave speeds and the polarization vectors $\mathbf{p}$ is obtained by eliminating $[\boldsymbol{\sigma}]$ from (A8):

$$(c^2\mathbf{M} - n_i\mathbf{B}_i\mathbf{C}n_j\mathbf{B}_j^T)[\mathbf{v}] = \mathbf{0}. \tag{A9}$$

The eigenvalues and eigenvectors of (A9) are the wave speeds (squared) and the polarization vectors $\mathbf{p}$. For wave propagation in the principal directions [100], [110], and [111], the wave speeds and polarization vectors are given in Table 4. To obtain the stress polarization vector note that (A8) gives

$$[\boldsymbol{\sigma}] = \frac{1}{c}\mathbf{C}n_i\mathbf{B}_i^T[\mathbf{v}]. \tag{A10}$$

Let $[\mathbf{v}] = \mathbf{p}$, be the polarization of the wave and let $[\boldsymbol{\sigma}] = \mathbf{S}$ denote the stress polarization vector. Then (A10) gives

$$\mathbf{S} = \frac{1}{c}\mathbf{C}n_i\mathbf{B}_i^T\mathbf{p}. \tag{A11}$$

Now

$$n_i\mathbf{B}_i^T = -\begin{pmatrix} n_1 & 0 & 0 \\ 0 & n_2 & 0 \\ 0 & 0 & n_3 \\ 0 & n_3 & n_2 \\ n_3 & 0 & n_1 \\ n_2 & n_1 & 0 \end{pmatrix} \quad , \quad n_i\mathbf{B}_i^T\mathbf{p} = -\begin{pmatrix} n_1p_1 \\ n_2p_2 \\ n_3p_3 \\ n_3p_2 + n_2p_3 \\ n_3p_1 + n_1p_3 \\ n_2p_1 + n_1p_2 \end{pmatrix} \tag{A12}$$

Then, the stress polarization vector for wave propagation along a principal direction in a cubic material is given by

$$\mathbf{S} = -\frac{1}{c}\begin{pmatrix} C_{11}n_1p_1 + C_{12}(n_2p_2 + n_3p_3) \\ C_{11}n_2p_2 + C_{12}(n_3p_3 + n_1p_1) \\ C_{11}n_3p_3 + C_{12}(n_1p_1 + n_2p_2) \\ C_{44}(n_2p_3 + n_3p_2) \\ C_{44}(n_3p_1 + n_1p_3) \\ C_{44}(n_1p_2 + n_2p_1) \end{pmatrix}. \tag{A13}$$

Appendix B: Kinematical Jump Condition

Continuity of displacement is required across the phase boundary in order to preclude separation, penetration and slip. Consider $\mathbf{u}(\mathbf{X}, t)$, the displacement at time t of the particle that was initially at $\mathbf{X}$ in the reference configuration. Continuity of $\mathbf{u}$ across the phase boundary requires the jump in the derivative of $\mathbf{u}$ along the propagating phase boundary to also be continuous across the phase boundary. Hence,

$$[\frac{du_i}{dt}]_b = [\frac{\partial u_i}{\partial t} + \frac{\partial u_i}{\partial X_j}\frac{dX_j}{dt}] = 0, \tag{B1}$$

where $\frac{dX_j}{dt} = c_p n_j$, for phase boundary normal $\mathbf{n}$ and velocity c_p. Then

$$[v_i] + c_p[\frac{\partial u_i}{\partial X_j}]n_j = 0. \tag{B2}$$

Hence, the jump in volocity across the propagating phase boundary is

$$[\mathbf{v}]_b = -c_p[\nabla \mathbf{u}]\mathbf{n} = -c_p[\mathbf{F} - \mathbf{I}]\mathbf{n}, \tag{B3}$$

where $\mathbf{F}$ is the deformation gradient tensor for the phase transformation.

Appendix C: Sensitivity of $\mathbf{p}^b$ to c_p

The resolved shear stress in region Q is given by

$$\tau^Q_{RSS} = \mathbf{d}^p \cdot \boldsymbol{\sigma}^Q \mathbf{n} = a^{4,3}\mathbf{d}^p \cdot \mathbf{S}^{4,3}\mathbf{n} + a^{3,2}\mathbf{d}^p \cdot \mathbf{S}^{3,2}\mathbf{n} + a^{2,1}\mathbf{d}^p \cdot \mathbf{S}^{2,1}\mathbf{n} \qquad (C1)$$

where $\boldsymbol{\sigma}^Q, \mathbf{S}^{i,j}$ denote the stress tensors whose representations as six-dimensional vectors are given in §3.1, 3.3. Consider the stress-strain relation depicted in Figure 9, relating the resolved shear stress on a habit plane to the corresponding component of shear strain. The slope of the $\tau - \gamma$ curve for the parent phase is G_{DO_3}. The slope of the $\tau - \gamma$ curve for the martensite phase is G_{18R}. The resolved shear stress in the transformed state satisfies

$$\tau^P_{RSS} - (\tau_{RSS})_C = (\rho_o c_p^2)(\gamma^P - \gamma^Q), \qquad (C2)$$

where $(\tau_{RSS})_C$ is the value of the resolved shear stress in front of the propagating phase boundary. Also,

$$\tau^P_{RSS} = G_{18R}(\gamma^P - \gamma_o), \qquad (C3)$$

where γ_o is the shear strain on the habit plane associated with the transformation from an unstressed parent phase. Therefore,

$$G_{18R}(\gamma^P - \gamma_o) - (\tau_{RSS})_C = (\rho_o c_p^2)(\gamma^P - \frac{(\tau_{RSS})_C}{G_{DO_3}}). \qquad (C4)$$

Rearrangement of terms gives

$$\gamma^P = \frac{G_{18R}\gamma_o + (\tau_{RSS})_C(1 - \frac{\rho_o c_p^2}{G_{DO_3}})}{(G_{18R} - \rho_o c_p^2)}. \qquad (C5)$$

Then

$$\gamma^P - \gamma^Q = \gamma^P - \frac{(\tau_{RSS})_C}{G_{DO_3}} = \frac{G_{DO_3}G_{18R}\gamma_o + (\tau_{RSS})_C(G_{DO_3} - G_{18R})}{G_{DO_3}(G_{18R} - \rho_o c_p^2)}. \qquad (C6)$$

The magnitude of the jump in velocity across the phase boundary in the direction $\mathbf{d}^p$ is

$$(c_p \mathbf{p}^b) \cdot \mathbf{d}^p = -c_p(\gamma^P - \gamma^Q). \qquad (C7)$$

Let $\hat{\mathbf{p}}^{\mathbf{b}}$ be the phase boundary polarization vector for the stress-free transformation and $\mathbf{p}^{\mathbf{b}} = \alpha\hat{\mathbf{p}}^{\mathbf{b}}$, then

$$-(\gamma^P - \gamma^Q) = \alpha\hat{\mathbf{p}}^{\mathbf{b}} \cdot \mathbf{d}^p = -\alpha\gamma_o. \tag{C8}$$

Therefore, $\alpha = \frac{\gamma^P - \gamma^Q}{\gamma_o}$ and the polarization vector of the phase boundary for the stressed material is

$$\mathbf{p}^{\mathbf{b}} = \frac{\gamma^P - \gamma^Q}{\gamma_o}\hat{\mathbf{p}}^{\mathbf{b}} = \frac{G_{DO_3}G_{18R}\gamma_o + (\tau_{RSS})_C(G_{DO_3} - G_{18R})}{G_{DO_3}(G_{18R} - \rho_o c_p^2)\gamma_o}\hat{\mathbf{p}}^{\mathbf{b}}. \tag{C9}$$

This expression indicates that $\mathbf{p}^{\mathbf{b}}$ depends weakly on c_p, particularly for the magnitudes of c_p expected for the projectile velocities considered in §4. For example, it is expected that the shear modulii will be of the order 10 GPa, and that $G_{DO_3} \simeq G_{18R}$. $(\tau_{RSS})_C$ is estimated to be appoximately 50 MPa, and γ_o approximately 0.1. Hence, the second term in the numerator is expected to be much smaller than the first term. Therefore, $\mathbf{p}^{\mathbf{b}} \simeq \hat{\mathbf{p}}^{\mathbf{b}}/(1 - \rho_o c_p^2/G)$, with $\rho_o c_p^2/G \ll 1$, for the phase boundary velocities expected. For this reason, the assumption in §4.3 that $\mathbf{p}^{\mathbf{b}}$ is independent of c_p, and is equal to the polarization vector in the unstressed material, appears reasonable.

variant	$[100]^m$	$[010]^m$	$[001]^m$
1	$\frac{1}{2}[011]$	$[\bar{1}00]$	$[0\bar{4}5]$
1′	$\frac{1}{2}[0\bar{1}\bar{1}]$	$[100]$	$[0\bar{5}4]$
2	$\frac{1}{2}[0\bar{1}1]$	$[\bar{1}00]$	$[0\bar{5}\bar{4}]$
2′	$\frac{1}{2}[0\bar{1}1]$	$[100]$	$[045]$
3	$\frac{1}{2}[101]$	$[0\bar{1}0]$	$[50\bar{4}]$
3′	$\frac{1}{2}[\bar{1}0\bar{1}]$	$[010]$	$[40\bar{5}]$
4	$\frac{1}{2}[10\bar{1}]$	$[0\bar{1}0]$	$[\bar{4}0\bar{5}]$
4′	$\frac{1}{2}[10\bar{1}]$	$[010]$	$[504]$
5	$\frac{1}{2}[110]$	$[00\bar{1}]$	$[\bar{4}50]$
5′	$\frac{1}{2}[\bar{1}\bar{1}0]$	$[001]$	$[\bar{5}40]$
6	$\frac{1}{2}[\bar{1}10]$	$[00\bar{1}]$	$[\bar{5}\bar{4}0]$
6′	$\frac{1}{2}[\bar{1}10]$	$[001]$	$[450]$

Table 1: Lattice Correspondences (Horikawa,et.al, 1988)

variant	$\mathbf{f}_1$	$\mathbf{f}_2$	$\mathbf{f}_3$
1	$\frac{1}{\sqrt{2}}[011]$	$[\bar{1}00]$	$\frac{1}{\sqrt{2}}[0\bar{1}1]$
1′	$\frac{1}{\sqrt{2}}[0\bar{1}\bar{1}]$	$[100]$	$\frac{1}{\sqrt{2}}[0\bar{1}1]$
2	$\frac{1}{\sqrt{2}}[0\bar{1}1]$	$[\bar{1}00]$	$\frac{1}{\sqrt{2}}[0\bar{1}\bar{1}]$
2′	$\frac{1}{\sqrt{2}}[0\bar{1}1]$	$[100]$	$\frac{1}{\sqrt{2}}[011]$
3	$\frac{1}{\sqrt{2}}[101]$	$[0\bar{1}0]$	$\frac{1}{\sqrt{2}}[10\bar{1}]$
3′	$\frac{1}{\sqrt{2}}[\bar{1}0\bar{1}]$	$[010]$	$\frac{1}{\sqrt{2}}[10\bar{1}]$
4	$\frac{1}{\sqrt{2}}[10\bar{1}]$	$[0\bar{1}0]$	$\frac{1}{\sqrt{2}}[\bar{1}0\bar{1}]$
4′	$\frac{1}{\sqrt{2}}[10\bar{1}]$	$[010]$	$\frac{1}{\sqrt{2}}[101]$
5	$\frac{1}{\sqrt{2}}[110]$	$[00\bar{1}]$	$\frac{1}{\sqrt{2}}[\bar{1}10]$
5′	$\frac{1}{\sqrt{2}}[\bar{1}\bar{1}0]$	$[001]$	$\frac{1}{\sqrt{2}}[\bar{1}10]$
6	$\frac{1}{\sqrt{2}}[\bar{1}10]$	$[00\bar{1}]$	$\frac{1}{\sqrt{2}}[\bar{1}\bar{1}0]$
6′	$\frac{1}{\sqrt{2}}[\bar{1}10]$	$[001]$	$\frac{1}{\sqrt{2}}[110]$

Table 2: Principal basis vectors for lattice deformation $\mathbf{U}^{\mathbf{d}}$

variant	n	$\mathbf{d^P}$
1(+)	[-0.68300,-0.71380,-0.15485]	[0.73041,-0.66752,-0.14458]
1(−)	[-0.68300,0.71380,0.15485]	[0.73041,0.66752,0.14458]
1′(+)	[0.68300,0.15485,0.71380]	[-.73041,0.14455,0.66753]
1′(−)	[0.68300,-0.15485,-0.71380]	[-.73041,-0.14455,-0.66753]
2(+)	[-0.68300,0.15485,-0.71380]	[0.73041,0.14455,-0.66753]
2(−)	[-0.68300,-0.15485,0.71380]	[0.73041,-0.14455,0.66753]
2′(+)	[0.68300,0.71380,-0.15485]	[-0.73041,0.66752,-0.14458]
2′(−)	[0.68300,-0.71380,0.15485]	[-0.73041,-0.66752,0.14458]
3(+)	[-0.15485,-0.68300,-0.71380]	[-0.14456,0.73041,-0.66753]
3(−)	[0.15485,-0.68300,0.71380]	[0.14456,0.73041,0.66753]
3′(+)	[0.71380,0.68300,0.15485]	[0.66753,-0.73041,0.14455]
3′(−)	[-0.71380,0.68300,-0.15485]	[-0.66753,-0.73041,-0.14455]
4(+)	[-0.71380,-0.68300,0.15485]	[-0.66753,0.73041,0.14455]
4(−)	[0.71380,-0.68300,-0.15485]	[0.66753,0.73041,-0.14455]
4′(+)	[-0.15485,0.68300,0.71380]	[-0.14456,-0.73041,0.66753]
4′(−)	[0.15485,0.68300,-0.71380]	[0.14456,-0.73041,-0.66753]
5(+)	[-0.71380,-0.15485,-0.68300]	[-0.66753,-0.14454,0.73041]
5(−)	[0.71380,0.15485,-0.68300]	[0.66753,0.14454,0.73041]
5′(+)	[0.15485,0.71380,0.68300]	[0.14457,0.66752,-0.73041]
5′(−)	[-0.15485,-0.71380,0.68300]	[-0.14457,-0.66752,-0.73041]
6(+)	[.15485,-0.71380,-0.68300]	[0.14457,-0.66752,0.73041]
6(−)	[-0.15485,0.71380,-0.68300]	[-0.14457,0.66752,0.73041]
6′(+)	[0.71380,-0.15485,0.68300]	[0.66753,-0.14454,-0.73041]
6′(−)	[-0.71380,0.15485,0.68300]	[-0.66753,0.14454,-0.73041]

Table 3: Habit plane normals (**n**) and the directions ($\mathbf{d^P}$) of the projection of shape deformation onto the habit plane.

mode	propagation direction, **n**	polarization vector, **p**	wave speed c	
longitudinal				
	[100]	[100]	$(c_{11}/\rho)^{1/2}$	4468 m/s
	$[111]/\sqrt{3}$	$[111]/\sqrt{3}$	$[(c_{11}+2c_{12}+4c_{44})/(3\rho)]^{1/2}$	6060 m/s
	$[110]/\sqrt{2}$	$[110]/\sqrt{2}$	$[(c_{11}+c_{12}+2c_{44})/2\rho]^{1/2}$	5704 m/s
transverse				
	[100]	$[0, p_2, p_3]$ (say [010],[001])	$[c_{44}/\rho]^{1/2}$ degenerate	3696 m/s
	$[111]/\sqrt{3}$	$[p_1, p_2, -(p_1+p_2)]$ (say $[1\bar{1}0]/\sqrt{2}$, $[11\bar{2}]/\sqrt{6}$)	$[(c_{11}-c_{12}+c_{44})/3\rho]^{1/2}$ degenerate	2298 m/s
	$[110]/\sqrt{2}$	$[1\bar{1}0]/\sqrt{2}$	$[(c_{11}-c_{12})/2\rho]^{1/2}$	1045 m/s
	$[110]/\sqrt{2}$	[001]	$[c_{44}/\rho]^{1/2}$	3696 m/s

Table 4: Principal directions for wave propagation in cubic crystals; wave speeds for Cu-14Al-4Ni (mass%).

RSS (MPa) : Normal Impact, n=[0.71380, 0.68300, 0.15485], Vo=35m/s									
	c_p=0m/s			c_p=2.5m/s			c_p=5m/s		
Variant	L (1)	T (2)	T (3)	L (1)	T (2)	T (3)	L (1)	T (2)	T (3)
1 (+)	4.29	10.02	12.52	4.29	9.76	15.70	4.29	9.51	18.87
1 (−)	-34.85	-29.61	-27.10	-34.83	-29.82	-23.87	-34.81	-30.04	-20.65
1′ (+)	3.25	7.87	9.67	3.25	7.66	11.92	3.24	7.46	14.17
1′ (−)	-15.51	-7.55	-6.08	-15.50	-7.90	-4.40	-15.50	-8.24	-2.73
2 (+)	27.84	21.29	21.92	27.82	21.57	23.06	27.81	21.84	24.20
2 (−)	25.24	22.60	22.87	25.23	22.70	23.35	25.22	22.80	23.84
2′ (+)	34.62	30.26	31.51	34.61	30.43	33.39	34.59	30.61	35.28
2′ (−)	0.17	-6.28	-4.87	0.17	-5.99	-2.66	0.17	-5.71	-0.45
3 (+)	1.93	6.91	5.18	1.93	6.69	2.58	1.93	6.47	-0.01
3 (−)	-16.50	-8.35	-9.70	-16.49	-8.70	-11.89	-16.48	-9.05	-14.07
3′ (+)	2.55	8.57	6.04	2.55	8.30	2.30	2.55	8.04	-1.43
3′ (−)	-36.51	-31.02	-33.39	-36.49	-31.25	-36.86	-36.47	-31.47	-40.32
4 (+)	33.98	29.33	27.95	33.96	29.52	26.25	33.94	29.71	24.54
4 (−)	-0.54	-7.23	-8.61	-0.54	-6.93	-10.21	-0.54	-6.64	-11.81
4′ (+)	27.55	20.83	20.18	27.54	21.11	19.57	27.52	21.39	18.97
4′ (−)	25.28	22.29	21.99	25.27	22.41	21.71	25.26	22.53	21.43
5 (+)	-62.21	-67.31	-67.97	-62.18	-67.06	-68.61	-62.14	-66.80	-69.25
5 (−)	-75.16	-75.89	-76.80	-75.12	-75.82	-77.98	-75.08	-75.75	-79.16
5′ (+)	-61.79	-66.83	-65.98	-61.76	-66.58	-64.56	-61.72	-66.32	-63.14
5′ (−)	-74.48	-75.28	-74.13	-74.44	-75.21	-72.48	-74.41	-75.14	-70.84
6 (+)	51.99	51.81	52.33	51.97	51.79	53.02	51.94	51.77	53.71
6 (−)	43.98	46.45	47.42	43.96	46.32	48.61	43.94	46.19	49.81
6′ (+)	51.63	51.34	50.51	51.60	51.33	49.36	51.58	51.32	48.21
6′ (−)	43.23	45.80	44.55	43.21	45.67	42.70	43.18	45.53	40.85

Table 5: Resolved Shear Stress for Normal Impact Loading.

RSS (MPa) : Pressure-Shear, n=[0.71380, 0.68300, 0.15485], θ=20 deg, Vo=30m/s									
	c_p=0m/s			c_p=2.5m/s			c_p=5m/s		
Variant	L (1)	T (2)	T (3)	L (1)	T (2)	T (3)	L (1)	T (2)	T (3)
1 (+)	3.46	11.12	-28.55	3.46	10.86	-25.37	3.46	10.61	-22.20
1 (−)	-28.10	-21.11	-60.88	-28.09	-21.32	-57.66	-28.07	-21.53	-54.43
1′ (+)	2.62	8.80	-19.62	2.62	8.59	-17.37	2.62	8.39	-15.12
1′ (−)	-12.51	-1.87	-25.21	-12.50	-2.21	-23.54	-12.49	-2.56	-21.86
2 (+)	22.45	13.70	3.68	22.44	13.97	4.82	22.42	14.25	5.97
2 (−)	20.36	16.82	12.45	20.34	16.93	12.93	20.33	17.03	13.41
2′ (+)	27.92	22.09	2.29	27.91	22.26	4.18	27.89	22.44	6.06
2′ (−)	0.14	-8.48	-30.74	0.14	-8.20	-28.53	0.14	-7.91	-26.33
3 (+)	1.56	8.22	35.69	1.56	7.99	33.09	1.56	7.77	30.50
3 (−)	-13.31	-2.42	18.85	-13.30	-2.77	16.66	-13.29	-3.12	14.47
3′ (+)	2.06	10.10	50.20	2.06	9.84	46.47	2.06	9.57	42.74
3′ (−)	-29.45	-22.11	15.40	-29.43	-22.33	11.93	-29.41	-22.56	8.47
4 (+)	27.40	21.19	43.07	27.39	21.38	41.37	27.37	21.57	39.67
4 (−)	-0.44	-9.38	12.51	-0.43	-9.08	10.92	-0.43	-8.79	9.32
4′ (+)	22.22	13.23	23.50	22.21	13.51	22.90	22.19	13.80	22.29
4′ (−)	20.39	16.39	21.02	20.38	16.51	20.74	20.36	16.63	20.46
5 (+)	-50.17	-57.00	-46.60	-50.14	-56.74	-47.24	-50.11	-56.48	-47.88
5 (−)	-60.62	-61.59	-47.14	-60.58	-61.52	-48.32	-60.54	-61.45	-49.50
5′ (+)	-49.83	-56.57	-70.04	-49.80	-56.32	-68.63	-49.77	-56.07	-67.21
5′ (−)	-60.07	-61.14	-79.36	-60.03	-61.07	-77.71	-60.00	-60.99	-76.06
6 (+)	41.93	41.68	33.46	41.91	41.66	34.15	41.88	41.65	34.85
6 (−)	35.47	38.77	23.45	35.45	38.64	24.65	35.43	38.51	25.84
6′ (+)	41.64	41.26	54.42	41.61	41.24	53.27	41.59	41.23	52.12
6′ (−)	34.86	38.30	58.13	34.84	38.17	56.28	34.82	38.03	54.43

Table 6: Resolved Shear Stress for Pressure-Shear Loading.

RSS (MPa) : Pressure-shear, n=[0.71380, 0.68300, 0.15485], θ=35 deg, Vo=20m/s									
	c_p = 0m/s			c_p = 2.5m/s			c_p = 5m/s		
Variant	L (1)	T (2)	T (3)	L (1)	T (2)	T (3)	L (1)	T (2)	T (3)
1 (+)	2.01	8.10	-37.33	2.01	7.84	-34.16	2.01	7.59	-30.98
1 (−)	-16.35	-10.79	-56.35	-16.33	-11.01	-53.13	-16.32	-11.22	-49.90
1′ (+)	1.52	6.43	-26.12	1.52	6.23	-23.87	1.52	6.02	-21.62
1′ (−)	-7.28	1.18	-25.56	-7.27	0.83	-23.89	-7.26	0.49	-22.21
2 (+)	13.06	6.11	-5.36	13.05	6.38	-4.22	13.04	6.66	-3.08
2 (−)	11.84	9.04	4.03	11.83	9.14	4.51	11.82	9.24	4.99
2′ (+)	16.25	11.61	-11.06	16.23	11.78	-9.18	16.21	11.96	-7.29
2′ (−)	0.08	-6.77	-32.27	0.08	-6.48	-30.06	0.08	-6.20	-27.85
3 (+)	0.91	6.20	37.66	0.91	5.98	35.07	0.91	5.75	32.47
3 (−)	-7.74	0.91	25.27	-7.73	0.56	23.08	-7.73	0.21	20.89
3′ (+)	1.20	7.59	53.52	1.20	7.32	49.79	1.20	7.06	46.05
3′ (−)	-17.13	-11.30	31.66	-17.12	-11.53	28.19	-17.10	-11.75	24.73
4 (+)	15.94	11.01	36.07	15.93	11.20	34.37	15.91	11.39	32.67
4 (−)	-0.25	-7.36	17.71	-0.25	-7.06	16.12	-0.25	-6.77	14.52
4′ (+)	12.93	5.79	17.55	12.92	6.07	16.95	12.90	6.35	16.34
4′ (−)	11.86	8.68	13.99	11.85	8.80	13.71	11.84	8.92	13.43
5 (+)	-29.19	-34.62	-22.71	-29.16	-34.36	-23.35	-29.13	-34.10	-23.99
5 (−)	-35.27	-36.04	-19.49	-35.23	-35.97	-20.67	-35.19	-35.90	-21.85
5′ (+)	-28.99	-34.35	-49.78	-28.96	-34.10	-48.36	-28.93	-33.84	-46.95
5′ (−)	-34.95	-35.80	-56.67	-34.91	-35.73	-55.02	-34.88	-35.66	-53.37
6 (+)	24.40	24.20	14.78	24.37	24.18	15.47	24.35	24.16	16.17
6 (−)	20.64	23.26	5.72	20.62	23.13	6.91	20.60	23.00	8.10
6′ (+)	24.23	23.92	39.00	24.20	23.91	37.85	24.18	23.90	36.70
6′ (−)	20.29	23.02	45.73	20.26	22.88	43.88	20.24	22.75	42.03

Table 7: Resolved Shear Stress for Pressure-shear Loading.

RSS (MPa) : Pressure-shear, n=[0.71380, 0.68300, 0.15485], θ=40 deg, Vo=20m/s									
	c_p = 0m/s			c_p = 2.5m/s			c_p = 5m/s		
Variant	L (1)	T (2)	T (3)	L (1)	T (2)	T (3)	L (1)	T (2)	T (3)
1 (+)	1.88	8.20	-42.92	1.88	7.95	-39.75	1.88	7.69	-36.58
1 (−)	-15.30	-9.52	-60.80	-15.28	-9.74	-57.57	-15.26	-9.95	-54.35
1′ (+)	1.43	6.53	-30.11	1.42	6.32	-27.86	1.42	6.12	-25.61
1′ (−)	-6.81	1.97	-28.12	-6.80	1.63	-26.44	-6.79	1.29	-24.77
2 (+)	12.22	5.00	-7.91	12.21	5.27	-6.77	12.19	5.55	-5.63
2 (−)	11.08	8.16	2.53	11.07	8.27	3.01	11.06	8.37	3.49
2′ (+)	15.20	10.38	-15.14	15.18	10.56	-13.25	15.17	10.73	-11.36
2′ (−)	0.08	-7.04	-35.74	0.08	-6.76	-33.53	0.08	-6.47	-31.32
3 (+)	0.85	6.34	41.76	0.85	6.12	39.16	0.85	5.90	36.57
3 (−)	-7.24	1.75	29.16	-7.24	1.39	26.97	-7.23	1.04	24.78
3′ (+)	1.12	7.76	59.45	1.12	7.50	55.72	1.12	7.23	51.99
3′ (−)	-16.03	-9.97	38.38	-16.01	-10.20	34.91	-15.99	-10.42	31.45
4 (+)	14.92	9.79	38.00	14.90	9.98	36.29	14.88	10.17	34.59
4 (−)	-0.24	-7.62	20.60	-0.24	-7.32	19.00	-0.24	-7.03	17.41
4′ (+)	12.10	4.67	17.92	12.08	4.96	17.31	12.07	5.24	16.71
4′ (−)	11.10	7.80	13.77	11.09	7.92	13.49	11.07	8.03	13.21
5 (+)	-27.31	-32.95	-19.55	-27.28	-32.69	-20.19	-27.25	-32.44	-20.83
5 (−)	-33.00	-33.80	-15.17	-32.96	-33.73	-16.35	-32.92	-33.66	-17.53
5′ (+)	-27.13	-32.69	-50.06	-27.10	-32.44	-48.64	-27.07	-32.19	-47.22
5′ (−)	-32.70	-33.58	-57.07	-32.66	-33.51	-55.42	-32.63	-33.44	-53.77
6 (+)	22.83	22.62	12.02	22.80	22.60	12.72	22.78	22.59	13.41
6 (−)	19.31	22.04	2.29	19.29	21.90	3.48	19.27	21.77	4.67
6′ (+)	22.67	22.35	39.32	22.64	22.34	38.17	22.62	22.33	37.02
6′ (−)	18.98	21.82	47.38	18.96	21.68	45.53	18.94	21.55	43.68

Table 8: Resolved Shear Stress for Pressure-shear Loading.

RSS (MPa) : Pressure-shear, n=[0.71380, 0.68300, 0.15485], θ=45 deg, Vo=20m/s									
	c_p = 0m/s			c_p = 2.5m/s			c_p = 5m/s		
Variant	L (1)	T (2)	T (3)	L (1)	T (2)	T (3)	L (1)	T (2)	T (3)
1 (+)	1.74	8.25	-48.19	1.74	7.99	-45.01	1.74	7.74	-41.84
1 (−)	-14.13	-8.18	-64.78	-14.11	-8.40	-61.56	-14.09	-8.61	-58.33
1′ (+)	1.32	6.57	-33.87	1.31	6.36	-31.62	1.31	6.16	-29.37
1′ (−)	-6.29	2.76	-30.46	-6.28	2.41	-28.79	-6.27	2.07	-27.11
2 (+)	11.29	3.85	-10.40	11.27	4.12	-9.26	11.26	4.40	-8.12
2 (−)	10.24	7.23	1.01	10.22	7.33	1.49	10.21	7.44	1.97
2′ (+)	14.04	9.08	-19.09	14.02	9.25	-17.21	14.01	9.43	-15.32
2′ (−)	0.07	-7.26	-38.93	0.07	-6.97	-36.73	0.07	-6.69	-34.52
3 (+)	0.78	6.44	45.53	0.78	6.22	42.94	0.78	6.00	40.34
3 (−)	-6.69	2.57	32.83	-6.68	2.22	30.64	-6.67	1.86	28.45
3′ (+)	1.03	7.88	64.93	1.03	7.61	61.20	1.03	7.34	57.47
3′ (−)	-14.81	-8.57	44.80	-14.79	-8.79	41.34	-14.77	-9.02	37.87
4 (+)	13.78	8.50	39.63	13.76	8.69	37.93	13.74	8.87	36.23
4 (−)	-0.22	-7.82	23.33	-0.22	-7.53	21.73	-0.22	-7.23	20.14
4′ (+)	11.17	3.53	18.15	11.16	3.81	17.54	11.15	4.09	16.94
4′ (−)	10.25	6.85	13.44	10.24	6.97	13.16	10.23	7.09	12.88
5 (+)	-25.23	-31.03	-16.24	-25.19	-30.77	-16.88	-25.16	-30.52	-17.52
5 (−)	-30.48	-31.31	-10.74	-30.44	-31.24	-11.92	-30.40	-31.17	-13.10
5′ (+)	-25.06	-30.79	-49.96	-25.02	-30.53	-48.54	-24.99	-30.28	-47.12
5′ (−)	-30.20	-31.11	-57.03	-30.17	-31.04	-55.39	-30.13	-30.97	-53.74
6 (+)	21.08	20.87	9.17	21.06	20.85	9.86	21.03	20.84	10.56
6 (−)	17.84	20.64	-1.16	17.81	20.51	0.03	17.79	20.38	1.23
6′ (+)	20.94	20.61	39.35	20.91	20.60	38.19	20.88	20.58	37.04
6′ (−)	17.53	20.45	48.67	17.51	20.32	46.82	17.49	20.18	44.97

Table 9: Resolved Shear Stress for Pressure-shear Loading.

RSS (MPa) : Pressure-shear, n=[0.71380, 0.68300, 0.15485], θ=40 deg, Vo=30m/s									
	c_p = 0m/s			c_p = 5m/s			c_p = 10m/s		
Variant	L (1)	T (2)	T (3)	L (1)	T (2)	T (3)	L (1)	T (2)	T (3)
1 (+)	2.82	12.31	-64.38	2.82	11.80	-58.04	2.82	11.29	-51.69
1 (−)	-22.95	-14.28	-91.19	-22.91	-14.71	-84.75	-22.88	-15.14	-78.30
1′ (+)	2.14	9.79	-45.16	2.13	9.38	-40.66	2.13	8.97	-36.16
1′ (−)	-10.22	2.96	-42.18	-10.20	2.27	-38.83	-10.18	1.59	-35.48
2 (+)	18.33	7.50	-11.87	18.31	8.05	-9.59	18.28	8.60	-7.31
2 (−)	16.62	12.25	3.79	16.60	12.45	4.76	16.57	12.66	5.72
2′ (+)	22.80	15.57	-22.70	22.77	15.92	-18.93	22.73	16.27	-15.16
2′ (−)	0.11	-10.56	-53.60	0.11	-9.99	-49.19	0.11	-9.42	-44.77
3 (+)	1.27	9.51	62.64	1.27	9.07	57.45	1.27	8.63	52.26
3 (−)	-10.87	2.62	43.74	-10.85	1.92	39.36	-10.83	1.21	34.99
3′ (+)	1.68	11.64	89.18	1.68	11.11	81.71	1.68	10.58	74.25
3′ (−)	-24.05	-14.96	57.56	-24.01	-15.41	50.63	-23.97	-15.86	43.70
4 (+)	22.38	14.69	57.00	22.34	15.06	53.59	22.31	15.44	50.18
4 (−)	-0.36	-11.43	30.90	-0.35	-10.84	27.71	-0.35	-10.25	24.51
4′ (+)	18.15	7.01	26.88	18.12	7.58	25.67	18.09	8.14	24.46
4′ (−)	16.65	11.69	20.66	16.62	11.93	20.09	16.60	12.17	19.53
5 (+)	-40.97	-49.42	-29.32	-40.91	-48.91	-30.60	-40.84	-48.40	-31.89
5 (−)	-49.50	-50.71	-22.76	-49.42	-50.57	-25.12	-49.35	-50.43	-27.47
5′ (+)	-40.69	-49.04	-75.09	-40.63	-48.53	-72.25	-40.57	-48.03	-69.42
5′ (−)	-49.05	-50.38	-85.60	-48.98	-50.23	-82.30	-48.90	-50.09	-79.01
6 (+)	34.24	33.93	18.03	34.19	33.90	19.42	34.14	33.86	20.80
6 (−)	28.97	33.05	3.43	28.92	32.79	5.82	28.88	32.53	8.20
6′ (+)	34.00	33.53	58.99	33.95	33.50	56.68	33.90	33.47	54.38
6′ (−)	28.47	32.73	71.07	28.43	32.46	67.37	28.38	32.19	63.67

Table 10: Resolved Shear Stress for Pressure-shear Loading.

Figure 1: Model of Structure Change : DO_3 to 18K

(Nishiyama and Kajiwara (1963); Otsuka, et.al. (1976))

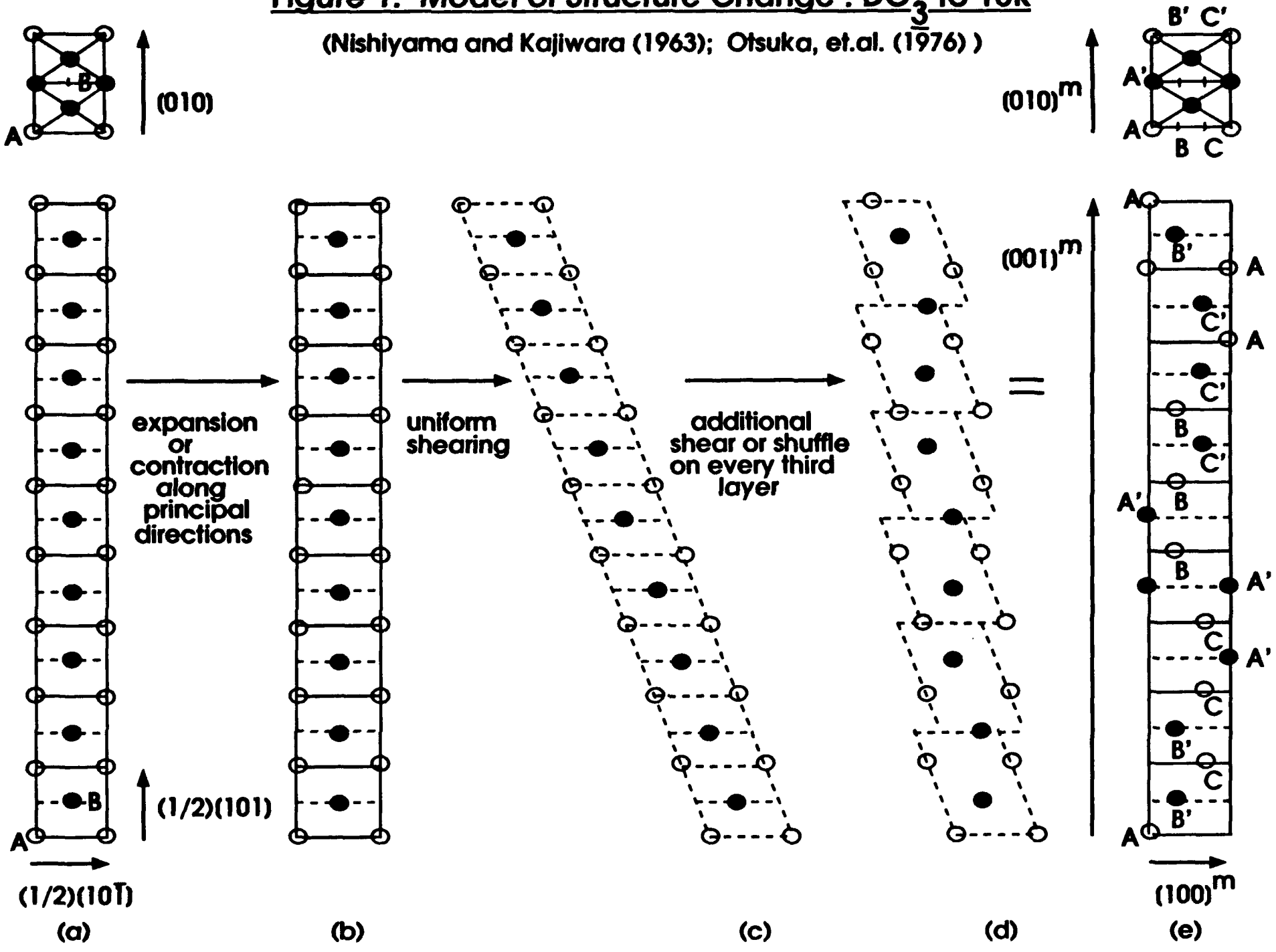

Figure 2: Approximated model of structure change: DO_3 to 18R

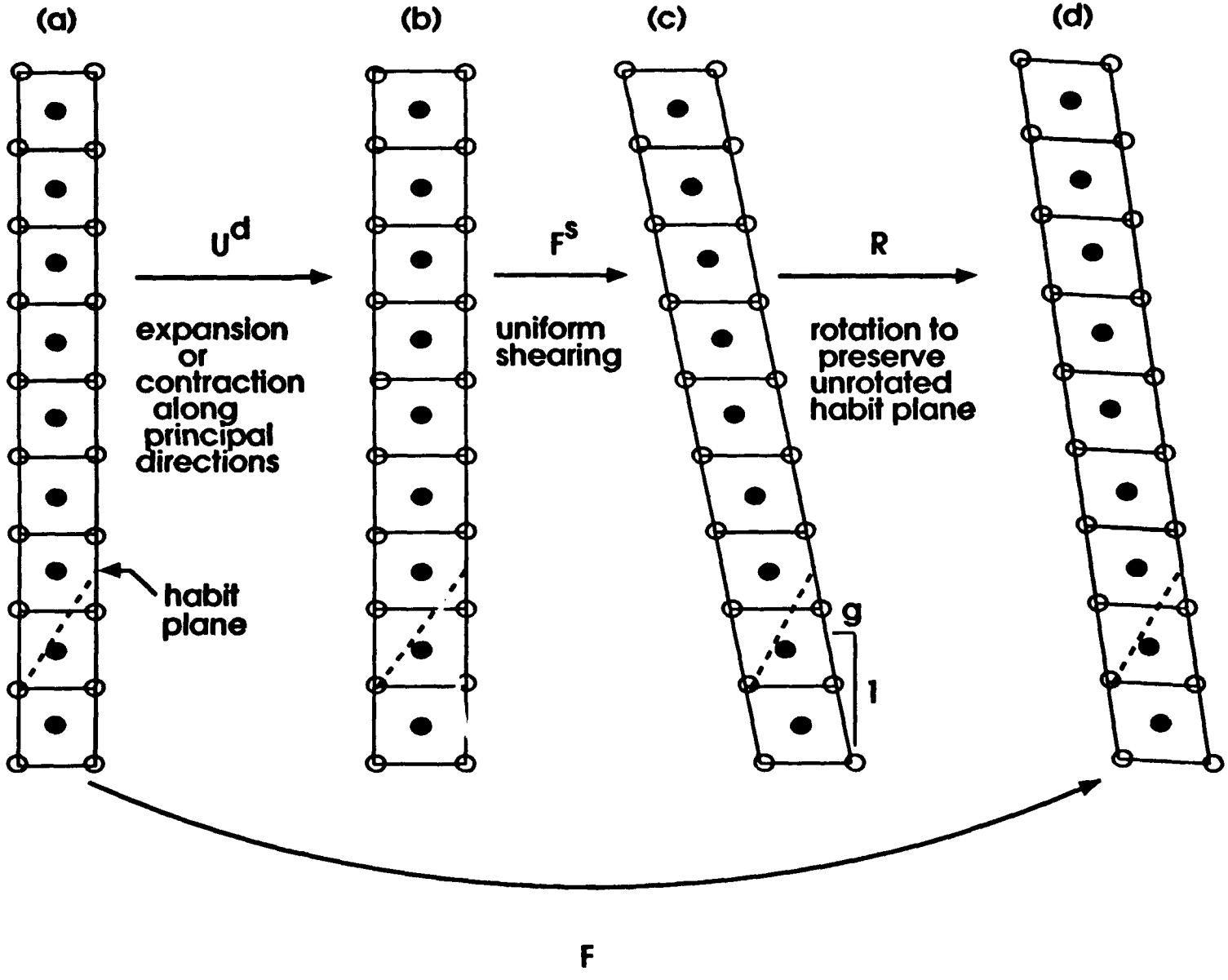

Figure 3: Symmetric Pressure-Shear Plate Impact

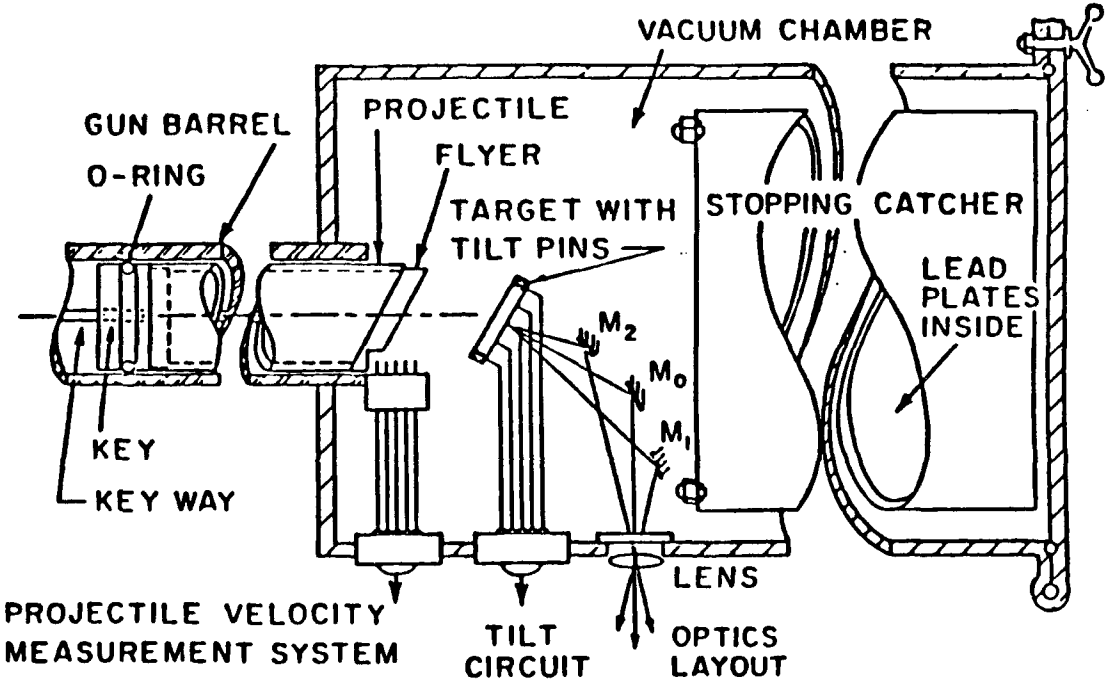

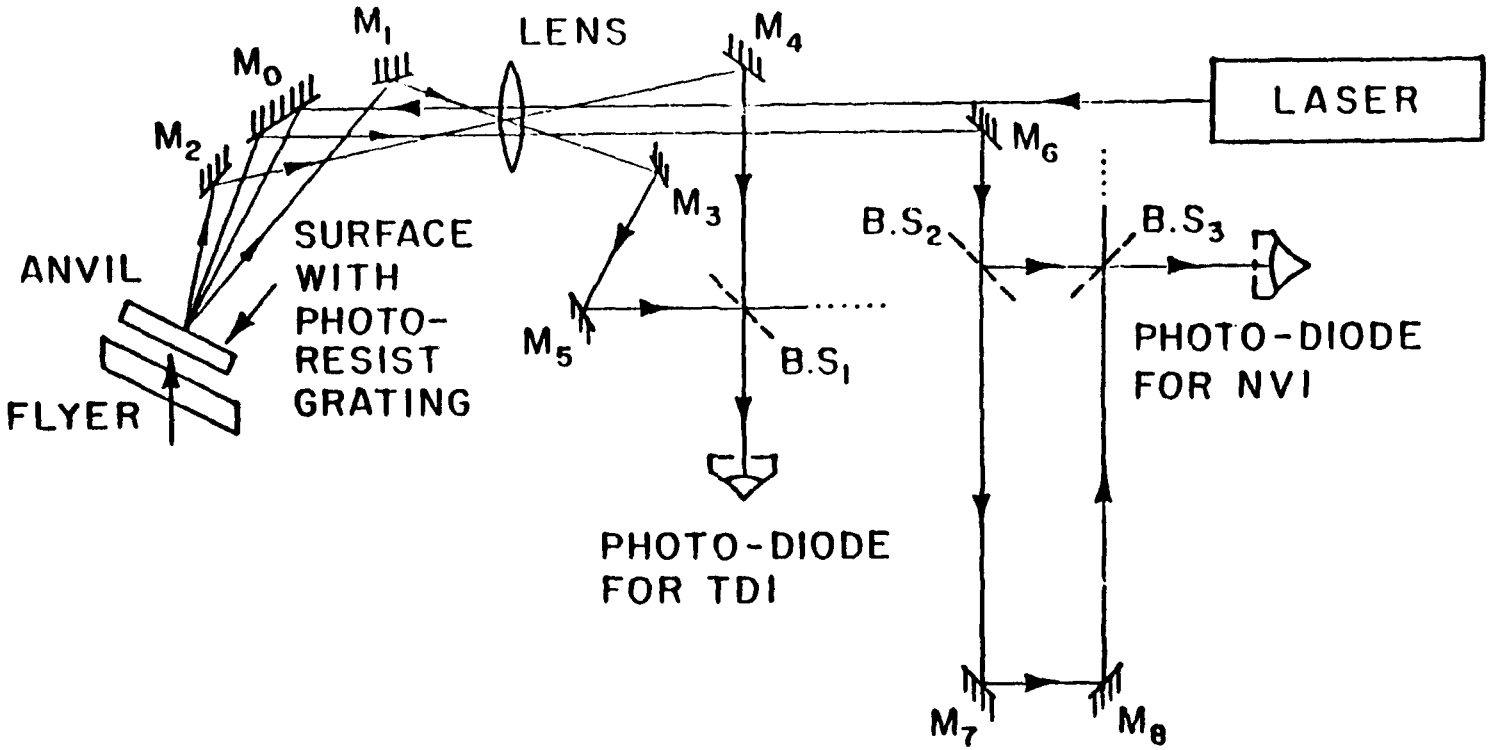

Figure 4: The Combined Normal Velocity and Transverse Displacement Interferometers

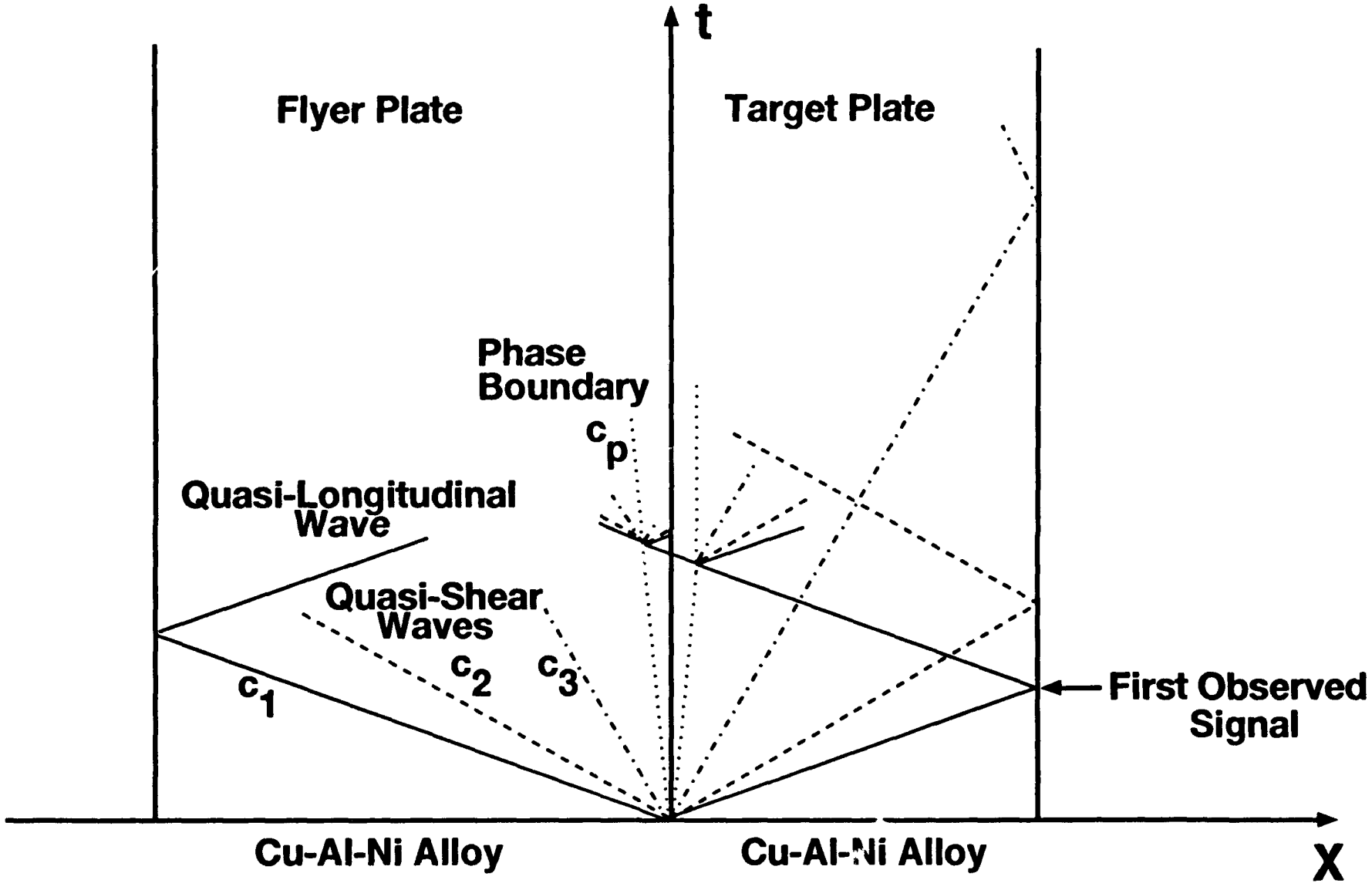

Figure 5: t-X Diagram

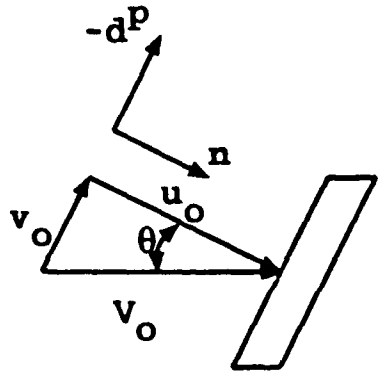

specimen orientation

(a)

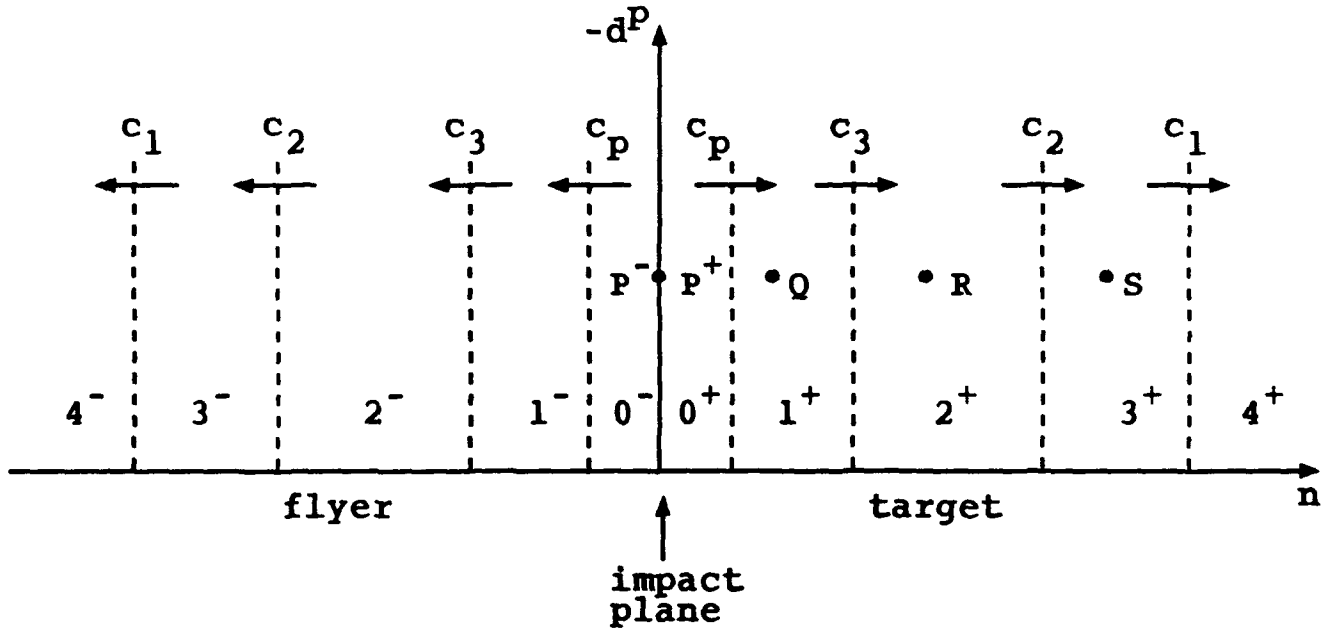

(b)

Figure 6

Figure 7: Resolved Shear Stress vs. Variant

θ=40deg., Vo=20m/s, cp=5m/s

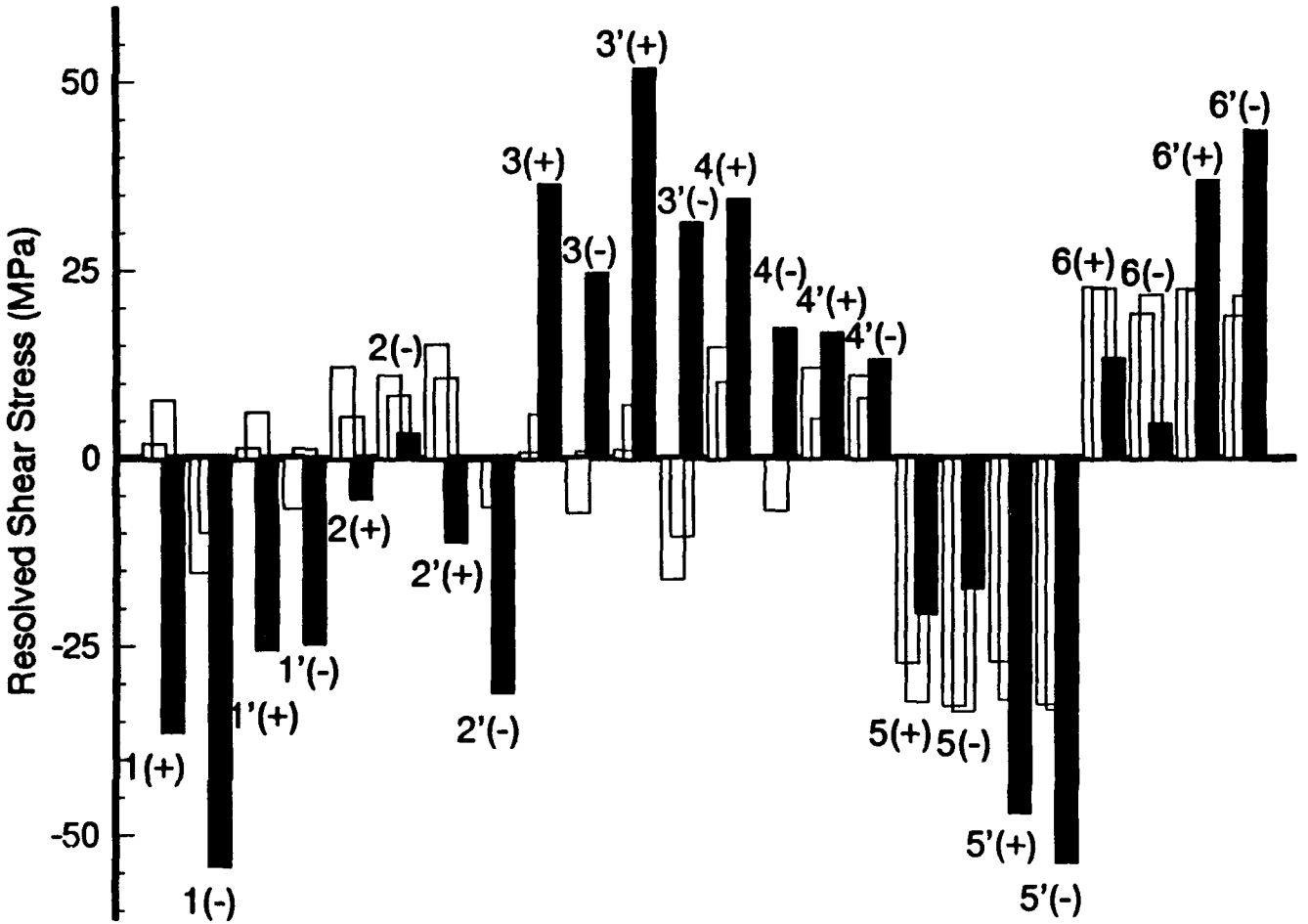

Figure 8: Velocity Jump Across Wavefront

θ=40deg., Vo=20m/s

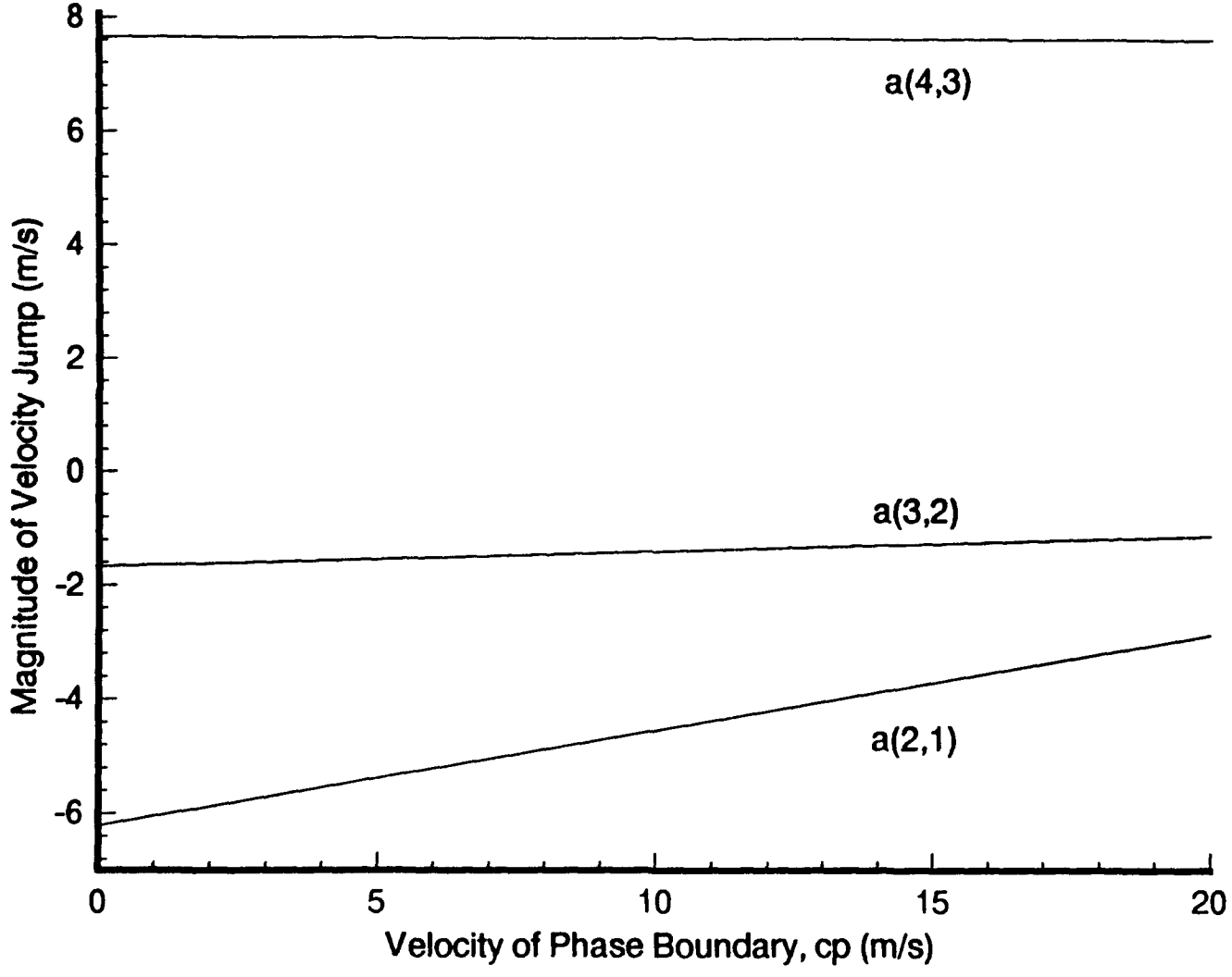

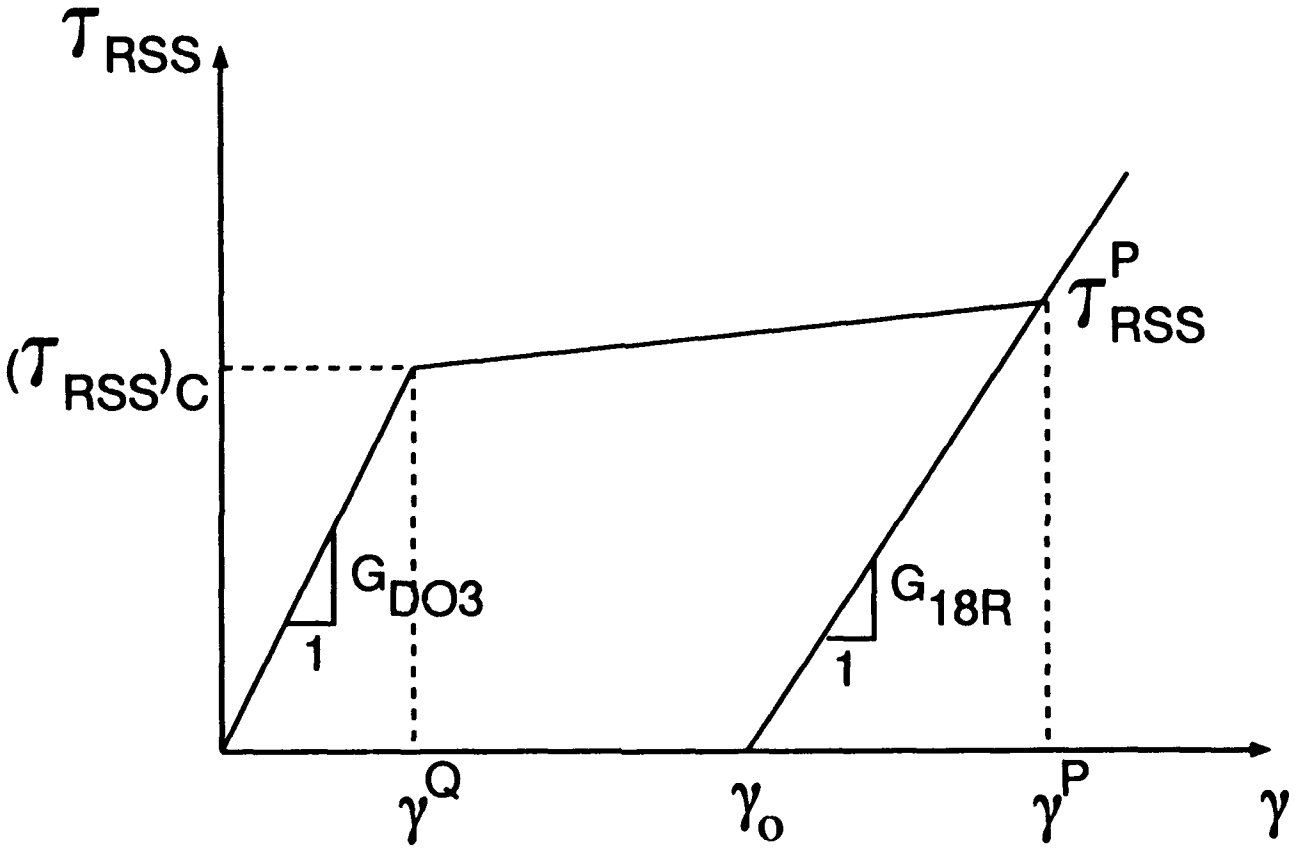

Figure 9: Stress-Strain Relation

Unclassified
SECURITY CLASSIFICATION OF THIS PAGE

REPORT DOCUMENTATION PAGE

Form Approved
OMB No. 0704-0188

1a. REPORT SECURITY CLASSIFICATION: Unclassified	1b. RESTRICTIVE MARKINGS
2a. SECURITY CLASSIFICATION AUTHORITY	3. DISTRIBUTION/AVAILABILITY OF REPORT: Unlimited
2b. DECLASSIFICATION/DOWNGRADING SCHEDULE	
4. PERFORMING ORGANIZATION REPORT NUMBER(S): Technical Report No. 1	5. MONITORING ORGANIZATION REPORT NUMBER(S)
6a. NAME OF PERFORMING ORGANIZATION: BROWN UNIVERSITY; 6b. OFFICE SYMBOL (If applicable)	7a. NAME OF MONITORING ORGANIZATION: Office of Naval Research
6c. ADDRESS (City, State, and ZIP Code): Division of Engineering, 182 Hope Street, Providence, RI 02912	7b. ADDRESS (City, State, and ZIP Code): Charles S. Draper Laboratory, 555 Technology Square MS54, Cambridge, MA 02139-3539
8a. NAME OF FUNDING/SPONSORING ORGANIZATION: Office of Naval Research; 8b. OFFICE SYMBOL (If applicable)	9. PROCUREMENT INSTRUMENT IDENTIFICATION NUMBER: N00014-91-J-4169
8c. ADDRESS (City, State, and ZIP Code): 800 N. Quincy St., Arlington, VA 22217-5000	10. SOURCE OF FUNDING NUMBERS: PROGRAM ELEMENT NO. / PROJECT NO. / TASK NO / WORK UNIT ACCESSION NO

11. TITLE (Include Security Classification)
"On Pressure-Shear Plate Impact for Studying the Kinetics of Stress-Induced Phase Transformations"

12. PERSONAL AUTHOR(S)
Joanne C. Escobar and Rodney J. Clifton

13a. TYPE OF REPORT	13b. TIME COVERED	14. DATE OF REPORT (Year, Month, Day)	15. PAGE COUNT
Technical	FROM _____ TO _____	July, 1992	45

16. SUPPLEMENTARY NOTATION

17. COSATI CODES			18. SUBJECT TERMS (Continue on reverse if necessary and identify by block number)
FIELD	GROUP	SUB-GROUP	Phase transformation, shape memory alloys, plate impact

19. ABSTRACT (Continue on reverse if necessary and identify by block number)

Pressure-shear plate impact experiments are proposed for studying the kinetics of stress-induced phase transformations. The purpose of this paper is to determine loading conditions and specimen orientations which can be expected to activate a single habit plane variant parallel to the impact plane, thereby simplifying the study of the kinetics of the transformation through monitoring the wave profiles associated with the propagating phase boundary. The Wechsler-Lieberman-Read phenomenological theory has been used to determine habit plane indices and directions of shape deformation for a Cu-Al-Ni shape memory alloy which undergoes a martensitic phase transformation under stress. Elastic waves generated by pressure-shear impact have been analyzed for wave propagation in the direction of the normal to a habit plane. A critical resolved shear-stress criterion has been used to predict variants which are expected to be activated for a range of impact velocities and relative magnitudes of the normal and transverse components of the impact velocity.

20. DISTRIBUTION/AVAILABILITY OF ABSTRACT	21. ABSTRACT SECURITY CLASSIFICATION
☒ UNCLASSIFIED/UNLIMITED ☐ SAME AS RPT. ☐ DTIC USERS	Unclassified
22a. NAME OF RESPONSIBLE INDIVIDUAL	22b. TELEPHONE (Include Area Code) / 22c. OFFICE SYMBOL

DD Form 1473, JUN 86 *Previous editions are obsolete.* SECURITY CLASSIFICATION OF THIS PAGE
Unclassified